LIGHT-WATER-REACTOR SAFETY
RESEARCH PROGRAM:
QUARTERLY PROGRESS REPORT

October—December 1979

ARGONNE
NATIONAL
LABORATORY

ARGONNE NATIONAL LABORATORY, ARGONNE, ILLINOIS

Prepared for the U. S. NUCLEAR REGULATORY COMMISSION

under Interagency Agreement DOE 40-550-75

8007180 031

ARGONNE NATIONAL LABORATORY
9700 South Cass Avenue
Argonne, Illinois 60439

LIGHT-WATER-REACTOR SAFETY
RESEARCH PROGRAM:
QUARTERLY PROGRESS REPORT
October–December 1979

by

Walter E. Massey, Laboratory Director
Jack A. Kyger, Associate Laboratory Director

Date Published: May 1980

Previous reports in this series

LIGHT-WATER-REACTOR SAFETY
RESEARCH PROGRAM:
QUARTERLY PROGRESS REPORT

October–December 1979

ABSTRACT

This progress report summarizes the Argonne National Laboratory work performed during October, November, and December 1979 on water-reactor-safety problems. The research and development areas covered are: (1) Heat Transfer Coordination for LOCA Research Programs and (2) Transient Fuel Response and Fission-product Release.

NRC FIN No.	FIN Title
A2014	Heat Transfer Coordination for LOCA Research Programs
A2016	Transient Fuel Response and Fission-product Release
A2017	Clad Properties for Code Verification
A2026	Phenomenological Modeling of Two Phase Flow in Water Reactor Safety

TABLE OF CONTENTS

LIGHT-WATER-REACTOR SAFETY
RESEARCH PROGRAM:
QUARTERLY PROGRESS REPORT

October–December 1979

EXECUTIVE SUMMARY

The objective of the study of transient critical heat flux (CHF) is to give a best-estimate recommendation of CHF during reactor transients and hypothetical accidents. To accomplish this task, we have developed a predictional method. Basically, this method involves the thermal-hydraulic calculation of the heated core with boundary conditions supplied from experimental measurements. Thermal-hydraulic calculations during LOCA were examined using both flow-driven and pressure-driven versions of the code. Some encouraging results were obtained for the flow driven calculations, as demonstrated by the good agreement with in-core measurements. The pressure-driven calculations, on the other hand, showed less satisfactory agreement with measurements; therefore this version was not recommended for subsequent CHF predictions in this study. CHF predictions were based on instantaneous "local-conditions" hypotheses, and eight correlations (consisting of round-tube, rod-bundle, and transient correlations) were tested against most recent blowdown heat-transfer test data obtained in major U. S. facilities.

Both CISE and Biasi correlations were found to be capable of predicting the early CHF of ~1 s. The Griffith-Zuber correlation is credited for its prediction of the delay CHF, which occurs in a more tranquil state with slowly decaying mass velocity. In many instances, the early CHF can be well correlated by the $x = 1.0$ criterion; this is certainly indicative of an annular-flow dryout-type crisis. The delay CHF was found to occur at near or above 80% void fraction, and the success of the modified Zuber pool-boiling correlation suggests that this CHF is caused by flooding and pool-boiling-type hydrodynamic crisis.

Models for the random diffusion of gas bubbles from the grains to the grain faces, and from the grain faces to the grain edges, were developed and included in the GRASS-SST analysis. Calculations made for TMI-2 accident-type (isothermal, low linear power) conditions show that the random diffusion of gas bubbles from the grains to the grain boundaries is a key factor influencing gas release under these conditions.

GRASS-SST analyses were performed for a calculated TMI-2 accident temperature scenario. The calculations were made for the fuel that reached the highest temperatures. Results indicate that ~42% of the generated gas has migrated out of the fuel grains to the grain faces and edges and is available to be released in the advent of extensive fuel fracturing. If no fuel

fracturing occurs, GRASS-SST predicts that this released intragranular gas remains trapped on the grain faces and grain edges.

Parametric analyses performed with GRASS-SST for various TMI-2 type fuel temperature and heating-rate scenarios show that most intragranular gas release occurs during the ramp, compared to a minor increase predicted to occur during a subsequent 5-h. high-temperature period. For given initial and final fuel temperatures, the analyses indicate that there is an optimum value of the heating rate for which the intragranular gas release will be a maximum.

Based on these analyses, if a substantial release of fission gas resulted as a consequence of the first 3 h of the accident at TMI-2, the following observations can be made:

The gas-bubble mobilities during some portion of the first 3 h must have been significantly higher (many orders of magnitude) than the diffusivities based on measurements made during similar isothermal conditions. Whether these mobilities resulted from a rapid heatup of the fuel, or from changes in stoichiometry, or both, or from some other unknown phenomenon is open to speculation at this time. In addition, extensive fuel fracturing must have occurred, enabling the gas that had reached the grain boundaries to vent to the exterior of the fuel.

I. HEAT TRANSFER COORDINATION FOR
LOCA RESEARCH PROGRAMS

Responsible Section Managers:
H. K. Fauske, R. E. Henry, and P. A. Lottes, RAS

A. Transient Critical Heat Flux (J. C. M. Leung, RAS)

1. More on Thermal-Hydraulic Calculations during Blowdown

A simple one-dimensional transient coolant-dynamic-analysis program, CODA, has been used to analyze the thermal-hydraulic behavior of an active core during LOCA conditions.[1] Some encouraging results were reported in Ref. 2, and more recent analyses are presented below.

a. Flow-driven Calculations

In general, the following boundary conditions are specified as input to the flow-driven version of CODA:

(1) System pressure

(2) Mass flow rate at either inlet or outlet

(3) Heat flux into coolant

(4) Fluid enthalpy at inflow boundary.

Conditions 1, 2, and 4 are usually referred to as the hydraulic boundaries; condition 3 is known as the thermal boundary. The first three conditions are inputted into CODA as time data/value pairs. At present the fourth boundary condition is specified within the code itself by simply treating the inflow enthalpy (at either inlet or outlet) to have the same value as the initial value; e.g., for a flow-reversal situation at the outlet of the core, the inflow enthalpy is taken to be at the initial outflow value. This treatment is adequate in most instances, but the code could be easily adapted to handle a specified inflow-enthalpy situation. Blowdown experiments conducted in two J. S. facilities were analyzed here, namely, the Semiscale Mod-3 facility[3] and the THTF facility.[4]

In the Semiscale Mod-3 facility, a full-length 5 x 5 PWR bundle was accommodated with in-core measurements consisting of numerous single-beam densitometers at various axial levels and a momentum-sensing drag-screen device at the bottom of the heated core. In addition, a drag screen and a turbine meter were installed in the upper plenum region just below the hot-leg outlet nozzle as shown in Fig. I.1. For Test S-07-3,[5] the lower drag-screen mass flow has to be adjusted in a manner as described in Ref. 2 so as to yield identical mass flow rate as sensed by the turbine meters in the downcomer and upper-plenum locations during steady-state conditions.

Elevation (cm)

444.5
432
406
356
330
292
190
152
140
122
102
51
38
25
0
-13
25
-51
-64
-90
-102
-114
-140
-406
-419
-445
-464
-495
-521
-546
-559
-572
-584
-597
-696.6

Downcomer
inlet annulus

Cold leg
inlet nozzles

Downcomer

FD-424

Downcomer
instrument spool
piece

NV-499
lower
drag
scr

Hot leg
outlet
nozzles

FV-1
core turbine
meter

NV-9
upper drag
screen

Heated Core

Lower plenum
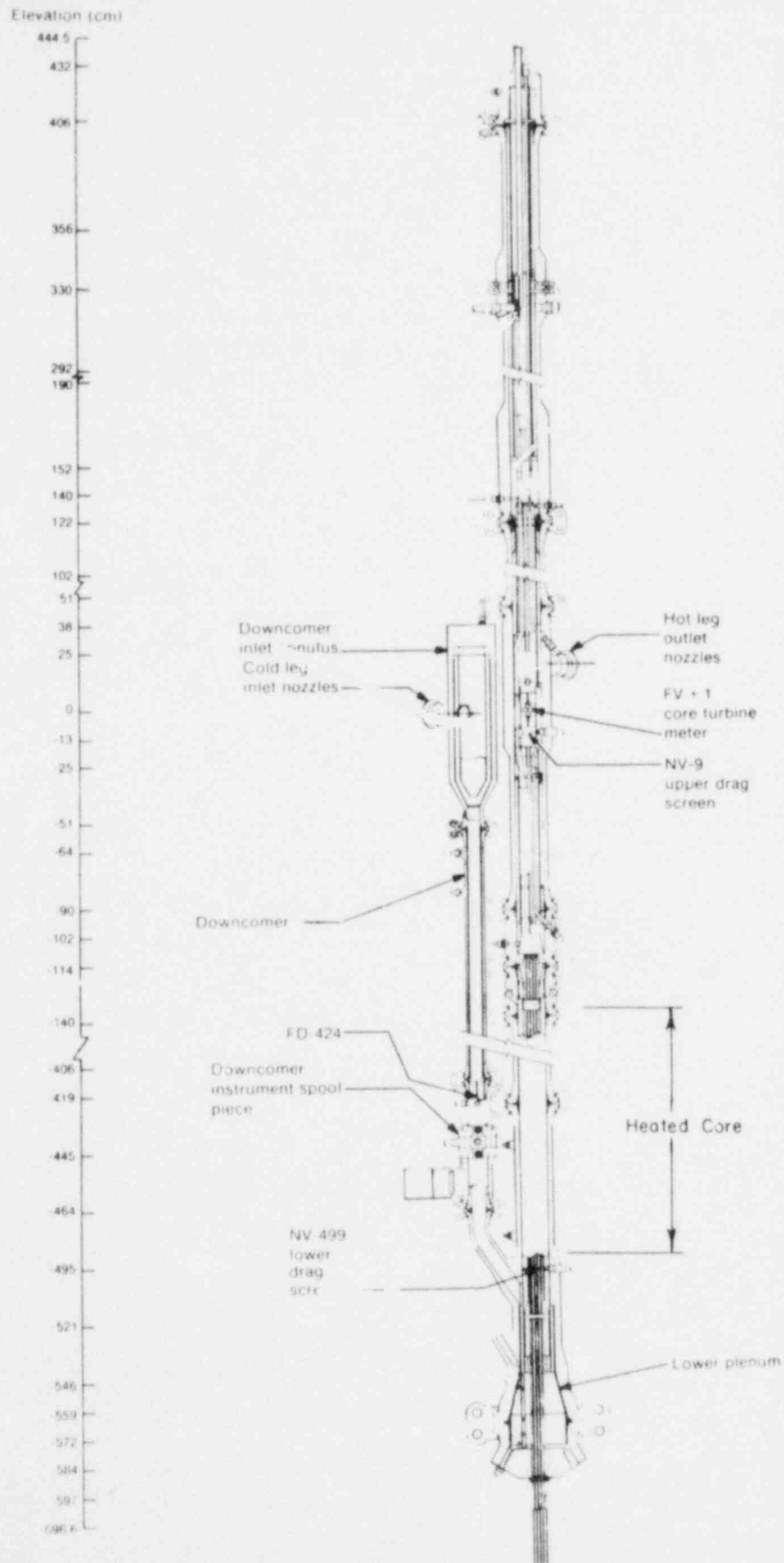
Fig. I.1. Cross Section of Semiscale Mod-3 Heater Core. ANL Neg. No. 900-80-55.

—

The resulting mass-flow data as shown in Fig. I.2 exhibits good agreement with the turbine-meter mass flow measured in the downcomer during the first 0.5 s into blowdown. This result therefore justifies the correction procedure, because during this period the liquid was still subcooled in the region between the lower core and the downcomer, and from the continuity equation,

$$A\frac{\partial \rho}{\partial t} + \frac{\partial}{\partial z}(GA) = 0 \qquad (1)$$

the temporal change of density is necessarily small in the liquid regime, implying that the mass flow rate is constant spatially. However, this is no longer true when the two-phase mixture arrived at the lower core; the $\partial \rho/\partial t$ term took on a large negative value, and the mass flow at the core inlet was substantially decreased as shown in Fig. I.2.

In the subsequent CODA calculation, the hydraulic boundary conditions were the system pressure and the adjusted drag-screen mass flow at the core inlet. Figure I.3 compares the calculated core inlet temperature versus the data; the latter was consistently
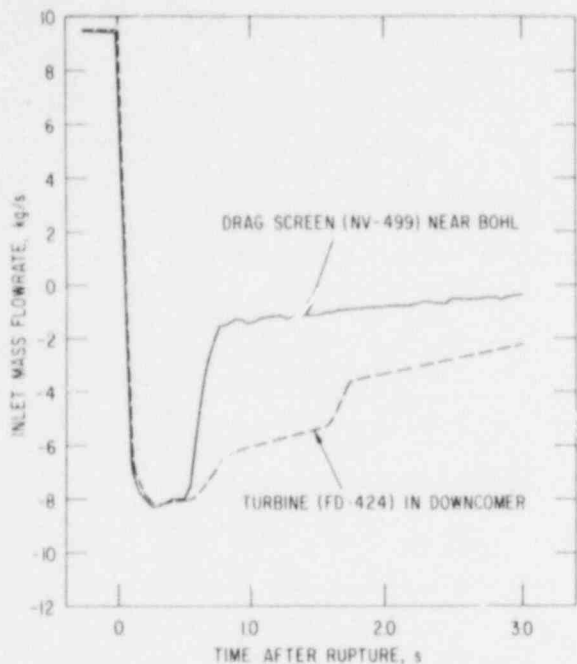
Fig. I.2. Comparison of Mass-flow Measurements at Core Inlet and External Downcomer in Semiscale Test S-07-3. ANL Neg. No. 900-80-172.
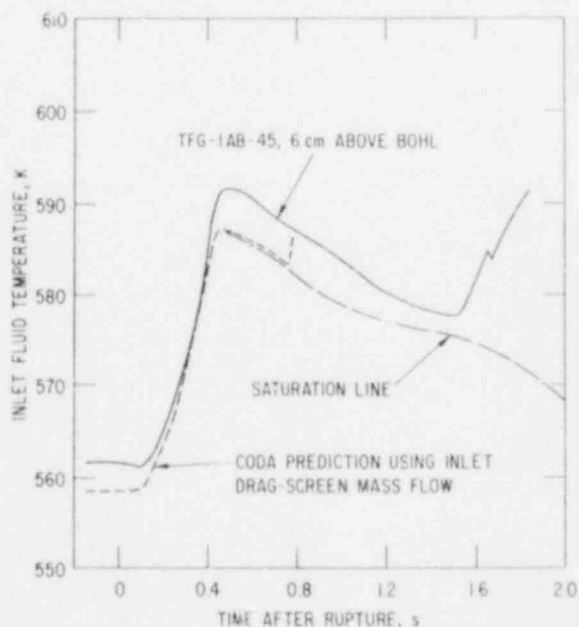
Fig. I.3

Prediction of Core-inlet Temperature in Semiscale Test S-07-3. ANL Neg. No. 900-80-18 Rev. 1.

4

higher, particularly during the saturated blowdown phase. Hence there appears to be a systematic error in the temperature measurement. Despite the apparent discrepancy, the data trend was well predicted during the first 800 ms. However, the code predicted superheat onset at about 0.8 s, as compared to 1.5 s observed experimentally. The predicted and calculated densities at the core inlet are compared in Fig. I.4, where generally good agreement is obtained.
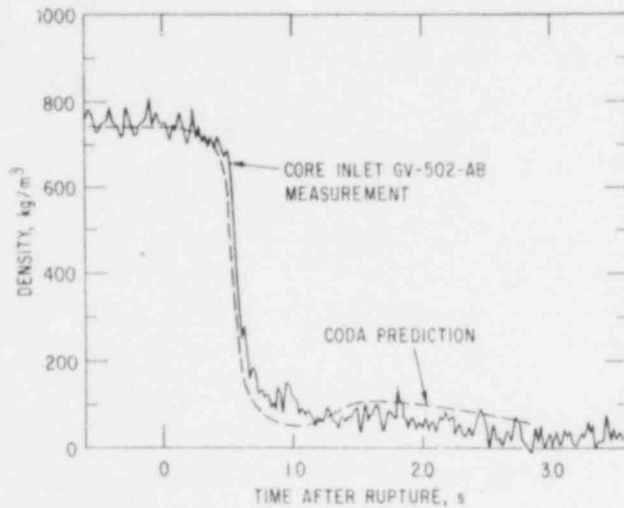
Fig. I.4. Prediction of Core-inlet Density in Semiscale Test S-07-3. ANL Neg. No. 900-80-139.

The calculated mass velocities at three levels in the heated core are illustrated in Fig. I.5, with outflow from the top and bottom of the core early in the transient, a bidirectional flow configuration. The upper core experienced a complete flow reversal only after 0.7 s. In the calculation, this reversal brought about an increase in fluid density (colder fluid) at the upper core as shown in Fig. I.6, and this behavior appears to be supported by the local density measurement.

Considerably improved instrumentation was achieved in Test S-07-9,[6] which exhibited similar core thermal behavior as in Test S-07-3. For this test, there was good agreement between the lower drag-screen mass
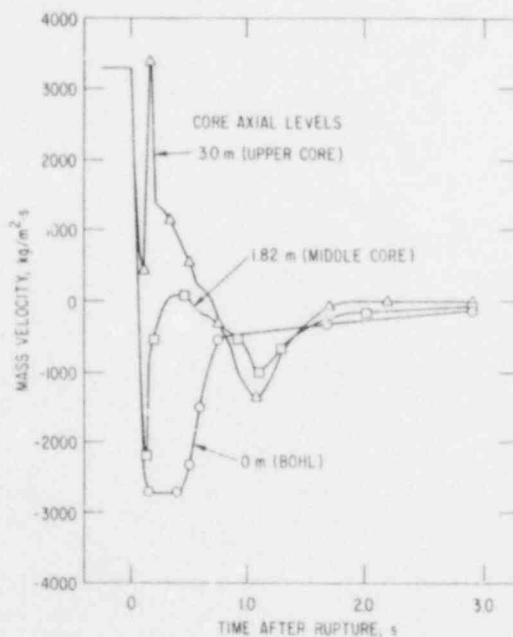
Fig. I.5. Calculated Mass-velocity Behavior in Semiscale Core for Test S-07-3. ANL Neg. No. 900-80-141.
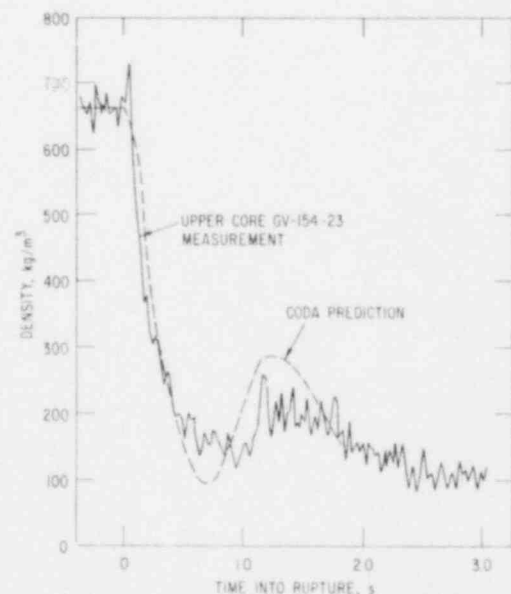
Fig. I.6. Comparison of Predicted Upper-core Density with Data for Semiscale Test S-07-3. ANL Neg. No. 900-80-122.

flow and other turbine-meter mass flow rates during steady-state operation. The calculated flow response in the upper plenum is compared with measured data in Fig. I.7, where good agreement was obtained for the early 700 ms. However, the large negative flow predicted at 1 s was not measured. The predicted core inlet density also exhibited good agreement with data in Fig. I.8.
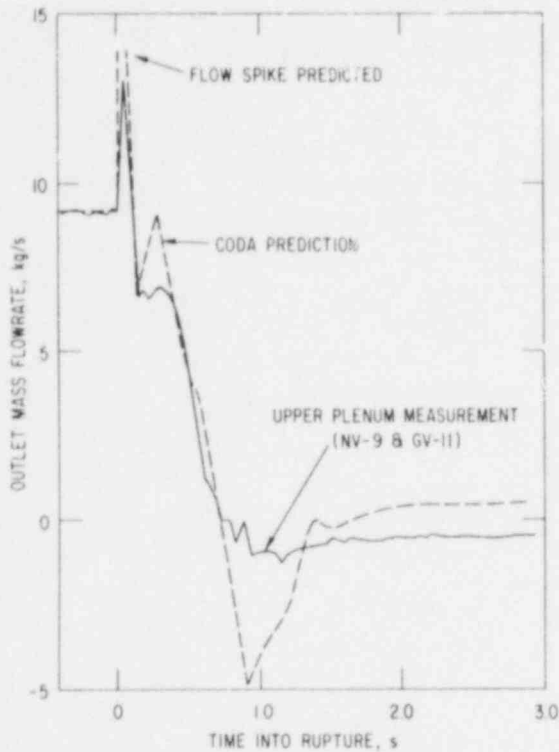
Fig. I.7. Prediction of Upper-plenum Flow Response for Semiscale Test S-07-9. ANL Neg. No. 900-80-170.
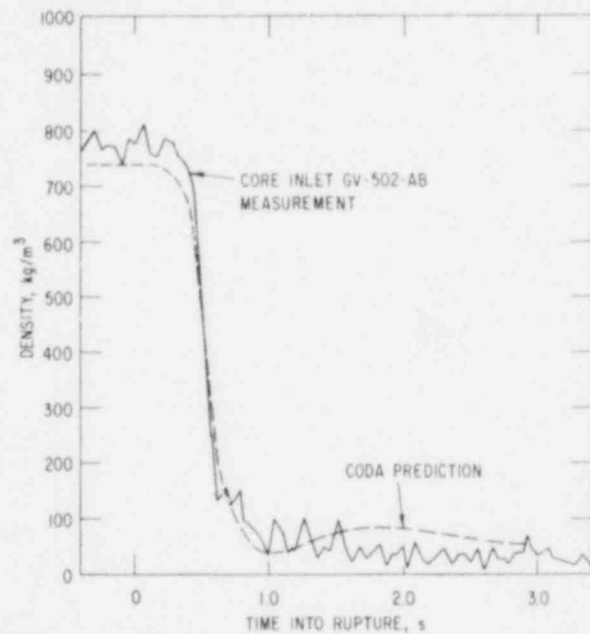
Fig. I.8. Prediction of Core-inlet Density for Semiscale Test S-07-9. ANL Neg. No. 900-80-143.

In the THTF blowdown facility, no in-core mass flow or density measurement was provided, while two instrumented spool pieces were installed immediately outside the pressure vessel; these are designated as vertical-inlet (VI) and vertical-outlet (VO) spool pieces (see Fig. I.9). Each spool piece consists of a densitometer, a bidirectional turbine flow meter, and a drag disk. Test 177,[7] currently regarded as an INEL code-verification test, was taken for analysis. It was conducted with a 32% inlet-28% outlet break. Two CODA calculations were performed, one driven by the VI drag-disk mass flow and the other driven by the VO turbine mass flow.

Figure I.10 illustrates the mass-flow behavior at the VO spool piece. The measured mass flow was positive (out of vessel) during the transient. The prediction follows the general trends of the measurement, but significantly more flow was predicted between 0.5 and 1.0 s. Because of the large volume of outlet piping and upper unheated core, the initiation of vaporization upon depressurization in the present equilibrium calculation gave rise to a

6

DC POWER

OUTLET

VO
SPOOL
PIECE

INLET

OUTFLOW

VI
SPOOL
PIECE

HEATED
CORE

INFLOW

7 X 7 PWR BUNDLE

A   A

SECTION A-A
ENLARGED VIEW
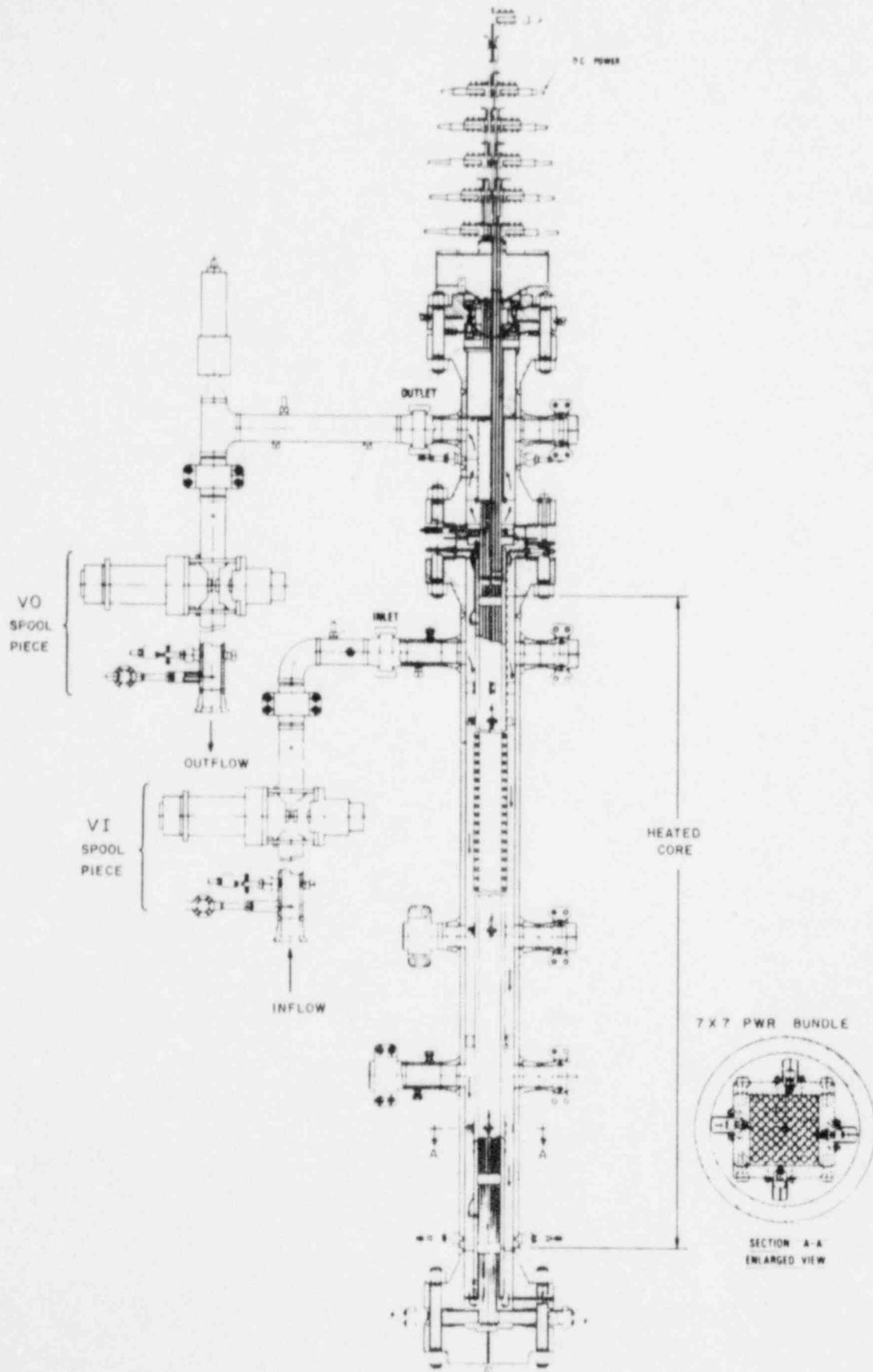
Fig. 1.9. Cross Section of THTF Bundle 1
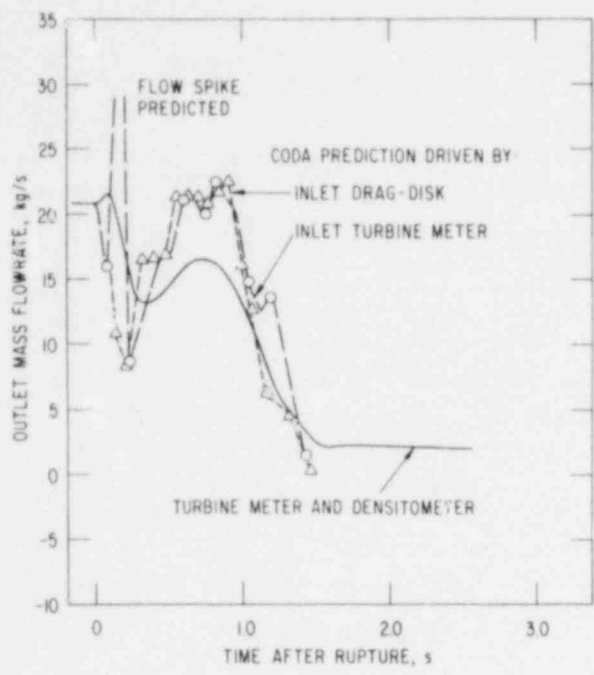
Fig. I.10

Mass-flow-rate Comparison at VO
Spool Piece for THTF Test 177.
ANL Neg. No. 900-80-150.

rapid expansion of the fluid in the outlet piping. This was observed in the
form of a flow spike as shown in Fig. I.10. Since this duration is rather short,
it is not expected to alter the core thermal hydraulic in any significant way.

Figure I.11 illustrates the mass-flow behavior at the VI spool
piece. The measured mass flow was initially positive (into the vessel), re-
versed quickly after rupture, and remained nearly steady from 1 to 3 s. The
prediction (based on CODA calculation driven by VO mass flow) was again
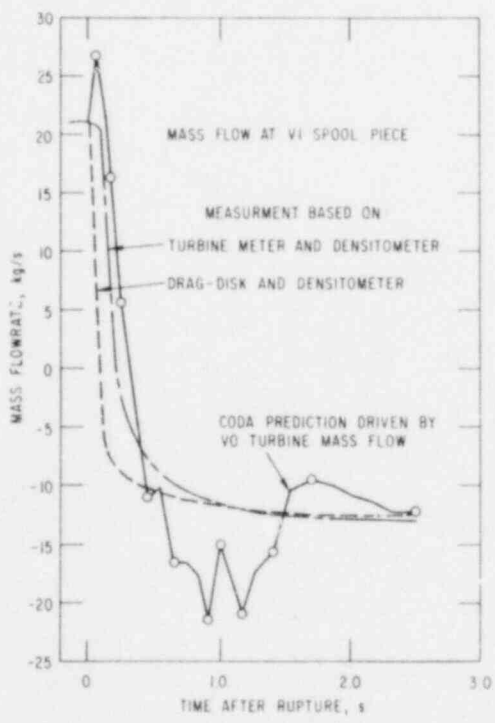
Fig. I.11

Mass-flow-rate Comparison at VI
Spool Piece for THTF Test 177.
ANL Neg. No. 900-80-38.

following the general trends of the data, but too much flow was predicted between 0.5 and 1.5 s. No explanation is apparent yet, but the results seem to suggest the importance of in-core mass-flow measurements in thermal-hydraulic evaluation; such measurements were unfortunately lacking in this facility.

In summary, some encouraging results have been obtained for thermal-hydraulic calculations during blowdown experiments as demonstrated by the good agreement with in-core measurements. Some difficulties were encountered with the drag-disk data, but a correction procedure has been suggested. It is also felt necessary to provide in-core mass-flow measurements for reliable thermal-hydraulic calculations and future verification purposes.

b.   Pressure-driven Calculations

The pressure-driven version has been developed in order to treat cases for which the pressure boundaries are measured with transducers. In Ref. 1, the present scheme was compared against the method-of-characteristic solution for one of the problems proposed by Hancox and Banerjee[8] with good results. However, in the present study, a number of limitations will be identified that will seriously affect the usefulness of such a scheme in thermal-hydraulic evaluation.

Snider[9] presented an analysis of Semiscale Mod-1 Test S-02-9 using the pressure-driven COBRA-IV-I version.[10] A similar calculation was performed here using CODA with boundary conditions governed by system pressure, pressure drop across the core, inflow enthalpy, and heat flux into coolant. The flow-area contraction between the core barrel inlet and the heated core, plus the expansion at the top of the heated core, were included in the model. Figure I.12 is a schematic of the core. Additional information regarding the loss coefficients (K factor) for grid spacers, flow-area change, drag-disk target and turbine-meter rotor have to be provided in this pressure-driven calculation. This loss coefficient is defined by the equation

$$K = \frac{2\rho\Delta P}{G^2} . \tag{2}$$

Presumably, these loss coefficients can be determined by a single-phase calibration procedure; such values were proposed by Snider.[9] The reported K values associated with the drag disk and turbine meter were 9.0 and 9.5, respectively, resulting in considerable pressure loss across these devices. For example, during steady-state flow, the pressure drop across these devices accounted for more than 25% of the total pressure drop. Hence, accurate determination of these coefficients is necessary.

In the present analysis, the K values were assumed to apply in the two-phase regime also, but this might not be true. Therefore it appears
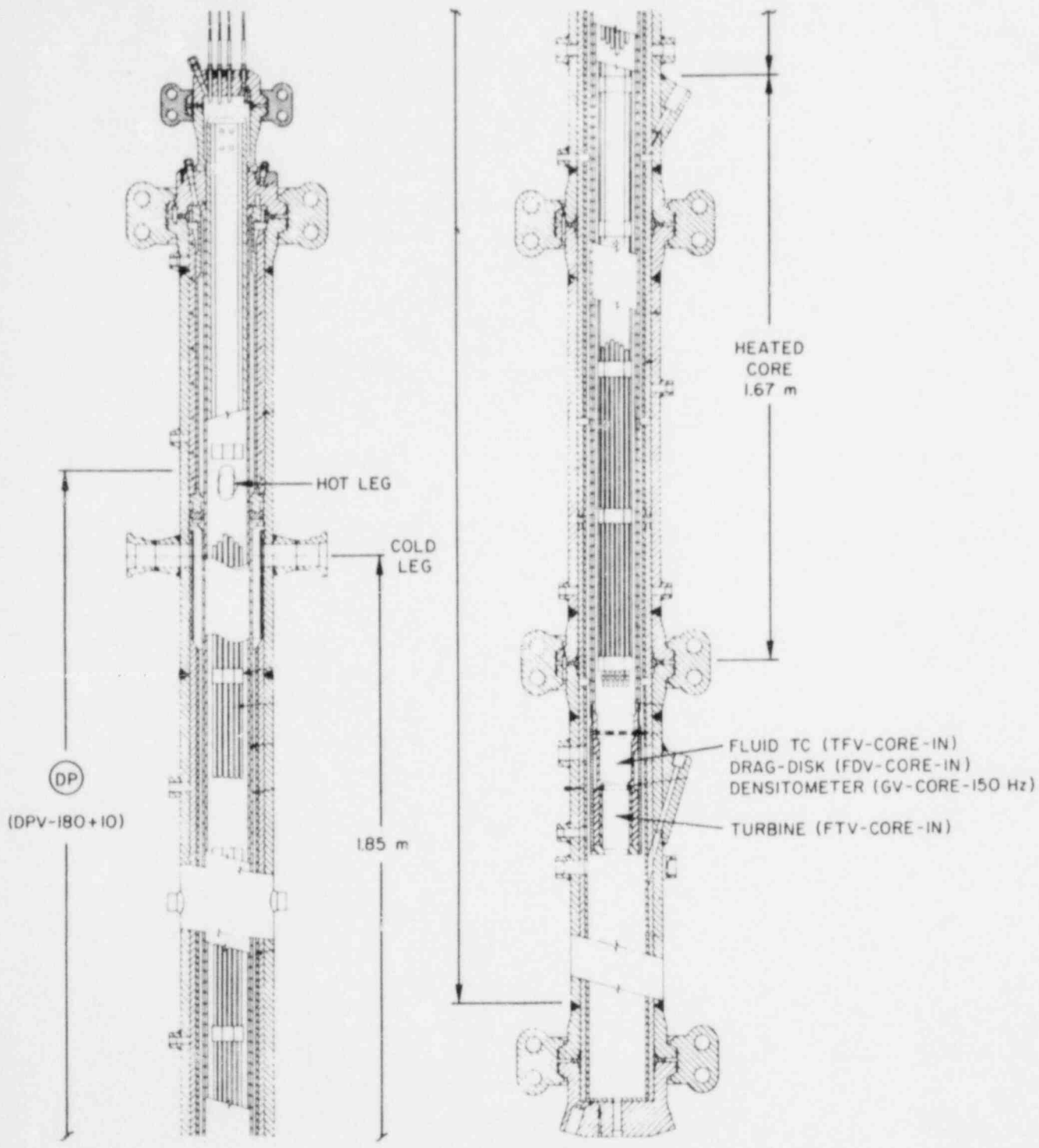
Fig. I.12. Location of Instruments Used to Measure Core-inlet Flow in Semiscale Mod-1 Facility. ANL Neg. No. 900-80-181.

that useful pressure-drop data should eliminate uncertainties caused by major flow-restriction devices. This in fact is closely approached in the Semiscale Mod-3 core. Figure I.13 compares the predicted mass flow at the core inlet to the measurements and Snider's result. CODA's prediction agrees well with Snider's COBRA-IV-I calculation. Both CODA and COBRA predicted significantly more negative flow than the drag-disk measurement during the first 0.4 s. Snider attributed this discrepancy to the mechanical limit reached by the drag disk. However, this is not confirmed by other test data obtained in the same facility; many such data had exceeded the apparent mechanical limit reported in Test S-02-9.

Fig. I.13. Comparison of Core-inlet Mass Velocity for Semiscale Test S-02-9. ANL Neg. No. 900-80-146.

The core-inlet-density behavior is illustrated in Fig. I.14. The CODA calculation predicted a slightly early decrease in density, whereas COBRA-IV-I predicted a slower response. A similar pressure-driven calculation was performed for Test S-28-1. Figure I.15 compares the predicted mass flow at core inlet with measurements. The prediction follows the general trend of the data,
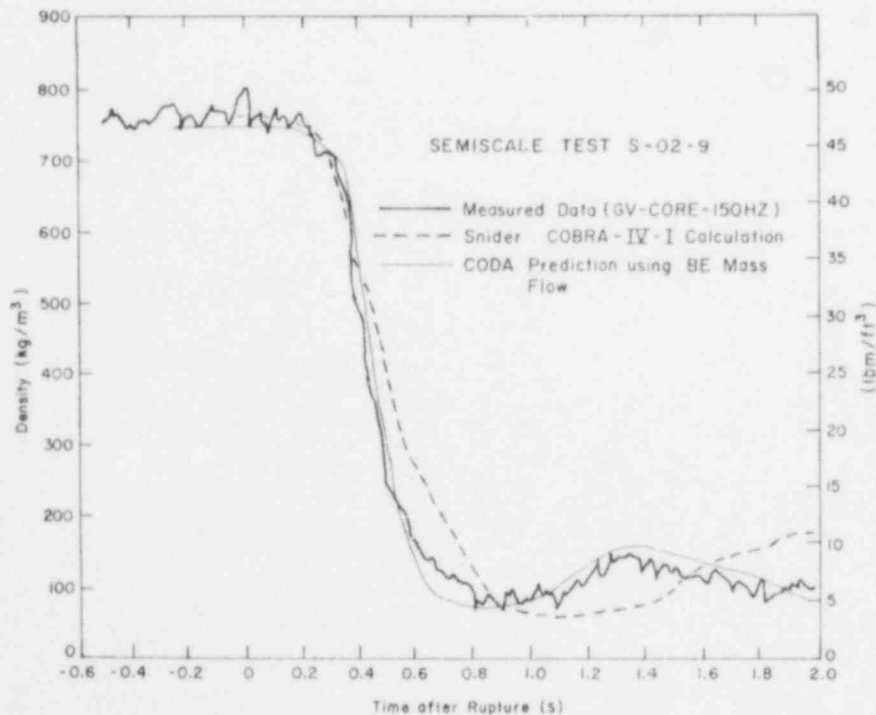
Fig. I.14. Comparison of Core-inlet Density Predicted by CODA Pressure-driven Calculation with Experimental Data. ANL Neg. No. 900-79-659.
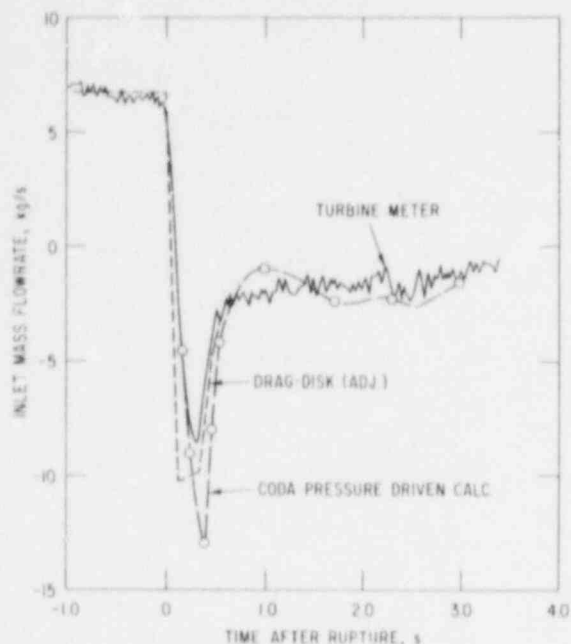
Fig. I.15. Comparison of Predicted Inlet Mass Velocity Using CODA Pressure-driven Scheme with Data for Semi-scale Test S-28-1. ANL Neg. No. 900-80-163.

but significant differences are observed. Again more negative flow was predicted at about 0.3 s, and the prediction lagged behind the response of the drag disk during the reversal period.

In the Semiscale Mod-3 core, a DP cell (DV-501-105) was installed to measure the pressure drop from -5.01- to -1.05-m elevation (with respect to the cold-leg nozzle), i.e., extending from the beginning of the heated core to 0.25 m above the active core. The flow area was essentially constant, except for the presence of 10 grid spacers and an inlet drag screen. The spacers were of similar design as the Mod-1 core, and the drag-screen target occupied about 34% of the flow area. The DP cell data from Test S-07-3 exhibited a great deal of ringing; consequently, a filtering procedure was performed by manually averaging the digital data every 0.085-s interval.

Two calculations were made using the "filtered" pressure-drop data: one with the appropriate loss coefficients (K = 0.56) for the spacers as given by Snider, and one without. The results of core-inlet mass-flow prediction are illustrated in Fig. I.16. The effect of the additional flow resistance as caused by spacers is seen to be minimal. During the interval between 0.3 and
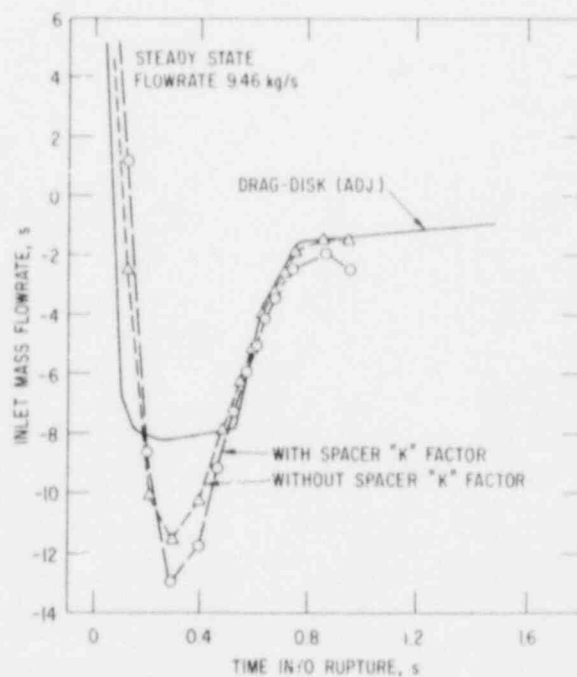
Fig. I.16

Calculated Core-inlet Mass Velocity Using CODA Pressure-driven Scheme for Semiscale Test S-07-3. ANL Neg. No. 900-80-138.

0.5 s, the calculation predicted significantly more negative flow than the drag-disk measurement. As shown in Fig. I.2, the latter measurement demonstrated close agreement with the mass-flow data taken at the external downcomer during this period.

In summary, the following observations can be made on pressure-driven CODA calculation:

(1) The prediction lags behind the response of drag-disk mass flow during the initial flow-reversal period.

(2) For Semiscale Mod-1 and Mod-3 cores, larger maximum downflow was predicted within the first 0.5 s.

Therefore the prediction is not at all satisfactory; the calculations were complicated by the presence of excessive ringing in the transducer line and uncertainty in defining the flow resistance of the drag disk, the turbine meter, spacers, and area change. For this reason, the pressure-driven CODA version was not used in CHF predictions in the present study.

2. CHF Predictions during Blowdown

In this section, the CHF-prediction results for various blowdown tests are discussed. The CHF data and prediction results are presented in the form of plots of axial elevation versus time. The conventional critical-heat-flux ratio (CHFR) is printed in CODA output at various locations for each CHF correlation. CHFR is a measure of the margin to CHF and is simply defined as

$$CHFR = \frac{Critical\ heat\ flux}{Local\ heat\ flux}. \tag{3}$$

Hence a CHFR value of less than 1.0 implies that CHF has been exceeded. In these plots the loci of CHFR = 1.0 are plotted; an example is given in Fig. I.17. The leading edge of the CHFR = 1.0 curve therefore represents the predicted CHF onset, but the trailing edge does not necessarily imply rewet or return to nucleate boiling (RNB). This is because other factors such as surface temperature and surface properties also play a major role in determining the rewet phenomena. Furthermore, for the case in which the surface heat flux is estimated by an inverse heat-conduction technique, the actual onset of CHF results in a much reduced heat flux, which can sometimes cause the CHFR to go above one. Since rewet is beyond the scope of the present study, the trailing edge in most cases was left incomplete, except in those cases for which later CHF was predicted.

Fig. I.17. Example of Plot of CHF Prediction. ANL Neg. No. 900-80-140.

In this quarterly report, prediction results are presented for the following blowdown tests:

THTF Tests 105, 104, 178, 181, and 177.

Semiscale Tests S-02-9, S-06-6, and S-07-3.

a. ORNL THTF Tests

Test 105 (Ref. 11) was conducted with a 50% inlet-60% outlet break configuration. The initial conditions in the 7 x 7 rod-bundle heated core were

P = 15.51 Pa,

T_{in} = 285°C,

$$W = 19.9 \text{ kg/s},$$

$$G = 3360 \text{ kg/m}^2 \cdot \text{s (in core)},$$

and

$$q = 6.0 \text{ MW (2.0 s into blowdown).}$$

The thermal-hydraulic calculation was made using the surface heat flux as determined by ORINC,[12] the measured system pressure, and the measured mass flow as determined from the turbine flowmeter and densitometer at the VI spool piece. The time to CHF, as determined from recorded sheath thermocouples, is shown in Fig. I.18, where the average times with one standard deviation are presented. The lower levels (below 2 m) incurred CHF uniformly, whereas the last two levels (levels I and J) exhibited two distinct onsets of CHF, resulting in a larger standard deviation.[13] As illustrated in Fig. I.18, the $x = 1.0$ line (i.e., complete liquid evaporation) appears to predict the early CHF data very well.
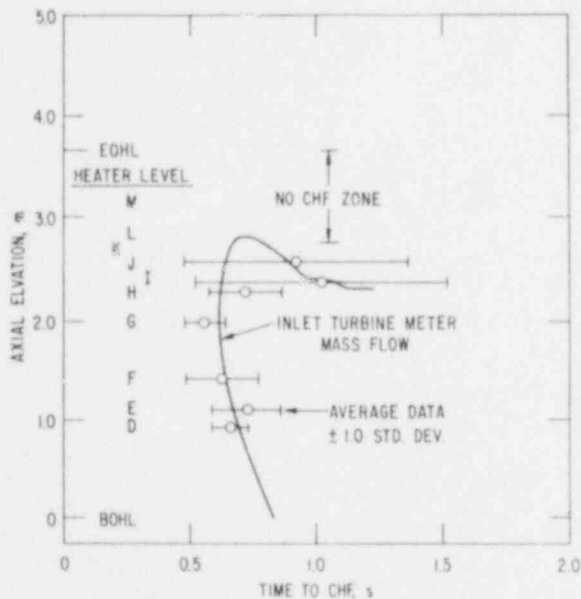
Fig. I.18

CHF Predictions Using $x = 1.0$ Criterion for THTF Test 105. ANL Neg. No. 900-80-35.

Test 104 (Ref. 13) was conducted with a 50% inlet-50% outlet break configuration. The initial conditions were

$$P = 15.5 \text{ MPa},$$

$$T_{in} = 287°C,$$

$$W = 20.0 \text{ kg/s},$$

$$G = 3340 \text{ kg/m}^2 \cdot \text{s (in core)},$$

and

$$q = 6.0 \text{ MW (2 s into blowdown).}$$

Hence Test 104 had similar initial conditions as Test 105, but with a larger inlet break size. As a result, Test 104 experienced stronger negative flow at the inlet spool piece, as shown in Fig. I.19. The surface-heat-flux results as reported in Ref. 12 were used as boundary conditions in CODA. The other supplied boundary conditions are the measured system pressure and the inlet-spool-piece mass flow.

The time-to-CHF data are shown in Fig. I.20, where two distinct CHF onsets were observed. Middle heater levels (I, J, K, and L) exhibited delay CHF at around 2 s, whereas the lower levels showed early CHF behavior. However, a number of thermocouples in these lower elevations did not measure early CHF. The uniformity of the heater-rod power (radially uniform) therefore precludes any significant three-dimensional thermal-hydraulic behavior that could be developed. The cause of this incoherent CHF onset is not presently understood.[14] Again the quality of the 1.0 criterion is shown in Fig. I.20 to do a remarkably good prediction of the early CHF behavior.

Fig. I.19

Comparison between Mass Flows for Tests 104 and 105 at VI Spool Piece. ANL Neg. No. 900-80-134.
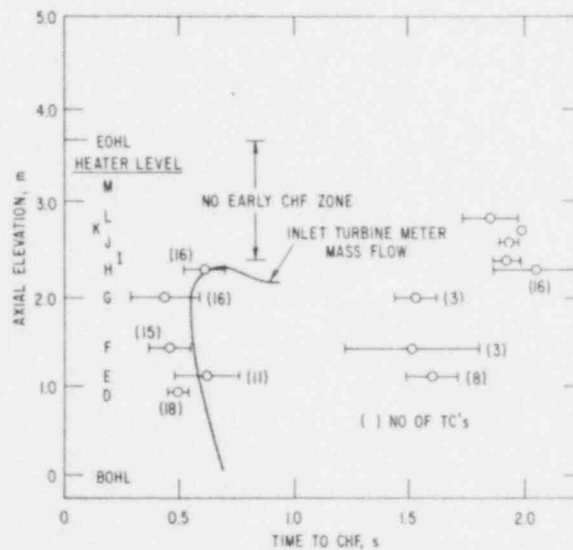
Fig. I.20

CHF Predictions Using x = 1.0 Criterion for THTF Test 104. ANL Neg. No. 900-80-24

Blowdown in Test 178 was accomplished by introducing a 32% inlet-28% outlet break with four unpowered rods.[15] The initial conditions were

$$P = 15.9 \text{ MPa},$$

$$T_{in} = 277°C,$$

$$W = 19.6 \text{ kg/s},$$

$$G = 3310 \text{ kg/m}^2 \cdot \text{s (in core)},$$

and

$$q = 3.7 \text{ MW}.$$

This is a relatively less severe blowdown transient as compared to Tests 105 and 104. Sheath thermocouples did not exhibit any significant cooling early in the transient. Therefore, as a first approximation, constant heat-flux values were used in the thermal-boundary input.

CODA calculation was performed using the measured pressure history in the core and the measured flow rate at the VI spool piece. The prediction results are shown in Figs. I.21 and I.22. Since only a limited number of thermocouple data were reported in Ref. 15, a statistical average and standard deviation calculation could not be performed. For this reason, each data point in these figures represents an individual thermocouple measurement. Flow was calculated to be expelled at each end of the heated core, and complete evaporation (x = 1.0) resulted in overheating of the heated bundle.
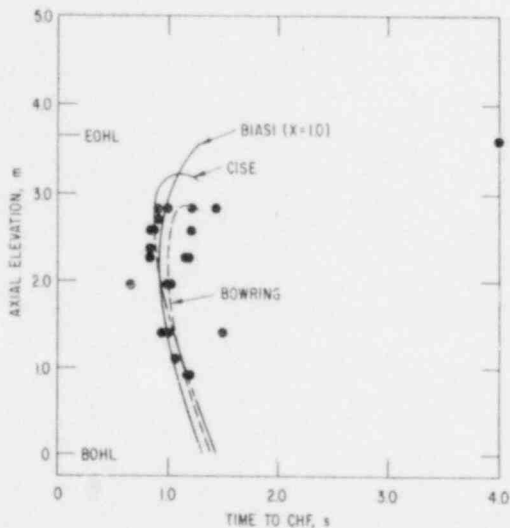
Fig. I.21. CHF Predictions Using Round–tube Correlations for THTF Test 178. ANL Neg. No. 900–80–125.
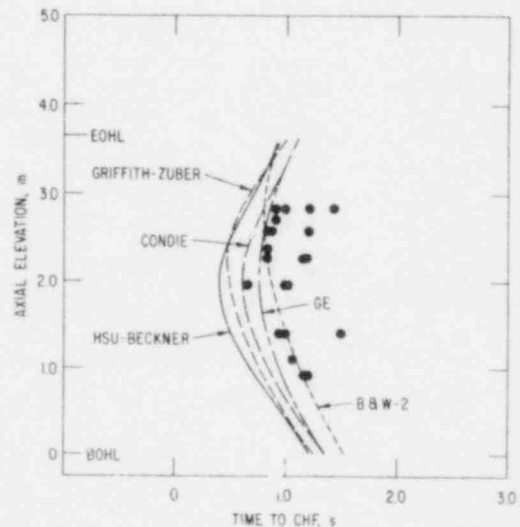
Fig. I.22. CHF Predictions Using Rod–bundle Correlations for THTF Test 178. ANL Neg. No. 900–80–124.

Test 181 was a mild transient with a 20% inlet break,[16] and the initial conditions were

$$P = 14.2 \text{ MPa},$$

$$T_{in} = 267°C,$$

$$W = 13.4 \text{ kg/s},$$

$$G = 2240 \ kg/m^2 \cdot s \ (in \ core),$$

and

$$q = 1.7 \ MW.$$

The core power was therefore more than three times lower than that in Test 105. During the transient, the system pressure dropped rapidly to about 6.9 MPa and remained at this level for some time (~3 s). Again the CODA calculation was performed using measured core pressure, mass flow rate at inlet spool piece, and constant heat flux at heater-rod boundary. The prediction results, as illustrated in Fig. I.23, indicate that Biasi and CISE correlations performed far better than the rod-bundle correlations. The 20% small inlet break led to a calculated fluid stagnation condition in the heated core, and eventually a high-quality two-phase mixture precipitated the observed CHF.
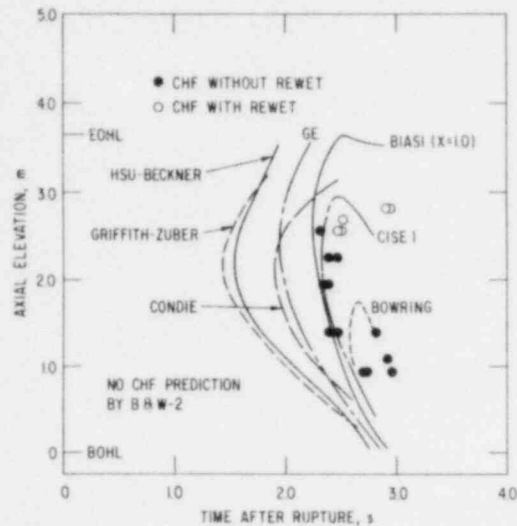
Fig. I.23. CHF Predictions for THTF Test 181. ANL Neg. No. 900-80-123.

Test 177 was conducted from the same initial conditions as in Test 178. The 32% inlet-28% outlet break was intended to simulate a 200% cold-leg break of a commercial PWR. Two CODA calculations were performed: one driven by the inlet drag-disk mass flow and the other driven by the outlet trubine-meter mass flow. In both cases, the surface heat flux was obtained from the ORINC inversion heat-conduction calculations.[17]

The prediction results of CISE and GE correlations are shown in Figs. I.24 and I.25, respectively, with good agreement with data. The x = 1.0 line also demonstrated to be an adequate prediction in Fig. I.26.

Fig. I.24

CHF Predictions Using CISE Correlation for THTF Test 177. ANL Neg. No. 900-80-29 Rev. 1.
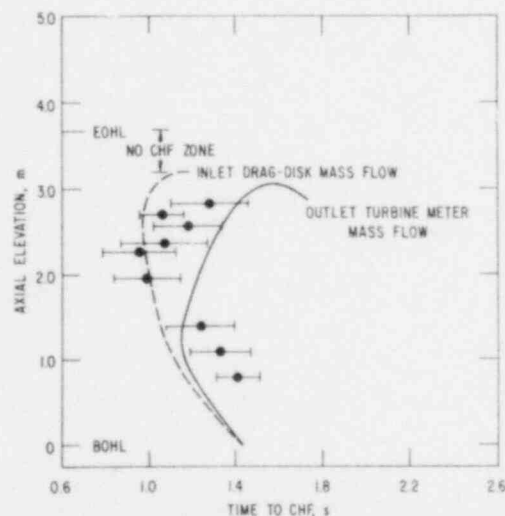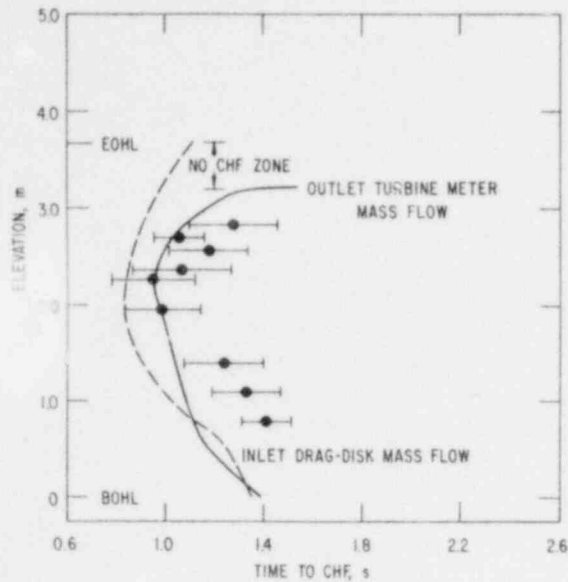
Fig. I.25. CHF Predictions Using GE Correlation for THTF Test 177. ANL Neg. No. 900-80-39 Rev. 1.
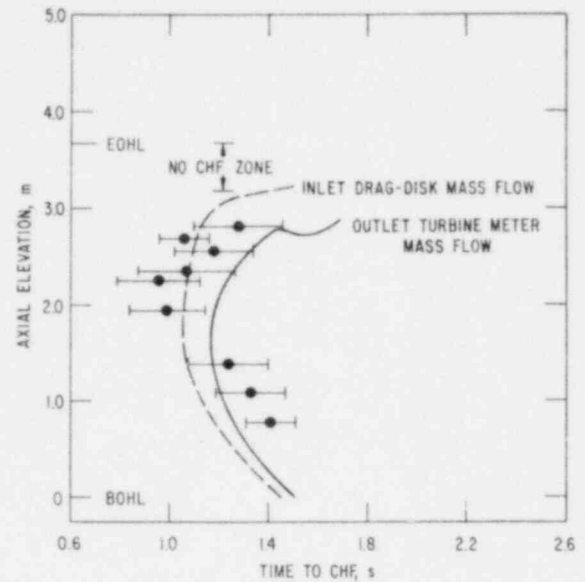
Fig. I.26. CHF Predictions Using Quality of 1.0 for THTF Test 177. ANL Neg. No. 900-80-26 Rev. 1.

b.   INEL Semiscale Tests

Semiscale Mod-1 Test S-02-9 was a 200% double-ended cold-leg break conducted from the initial conditions[18]

$$P = 15.5 \text{ MPa},$$
$$T_{in} = 283°C,$$
$$W = 7.35 \text{ kg/s},$$
$$G = 1440 \text{ kg/m}^2 \cdot \text{s (in core)},$$

and

$$q = 1.56 \text{ MW}.$$

Three were unpowered rods, and the remaining 37 rods had a peak power density of 38.8 kW/m. CHF was detected in the lower half of the core between 0.6 and 0.7 s, with most of the rods exhibiting rewet behavior above the 0.76-m (30-in.) elevation. The CHF predictions by various correlations are shown in Figs. I.27-I.29. Biasi, CISE, and B&W-2 correlations are seen to predict the data well; GE, Condie, Hsu-Beckner, and Griffith-Zuber correlations tend to underpredict the time.

Test S-06-6,[19] the last test in the Semiscale LOFT Counterpart Series, was a 200% double-ended cold-leg break initiated from the following steady-state conditions:

$$P = 15.8 \text{ MPa},$$
$$T_{in} = 290°C,$$
$$W = 4.9 \text{ kg/s},$$
$$G = 1020 \text{ kg/m}^2 \cdot \text{s (in core)},$$

and

$$q = 1.0 \text{ MW}.$$

This test was conducted with four central high-power rods at 39 kW/m peak power density, 32 at 24.7 kW/m, and four unpowered. In spite of this radial peaking profile, a one-dimensional thermal-hydraulic calculation was performed in an attempt to see how close a prediction could be achieved.
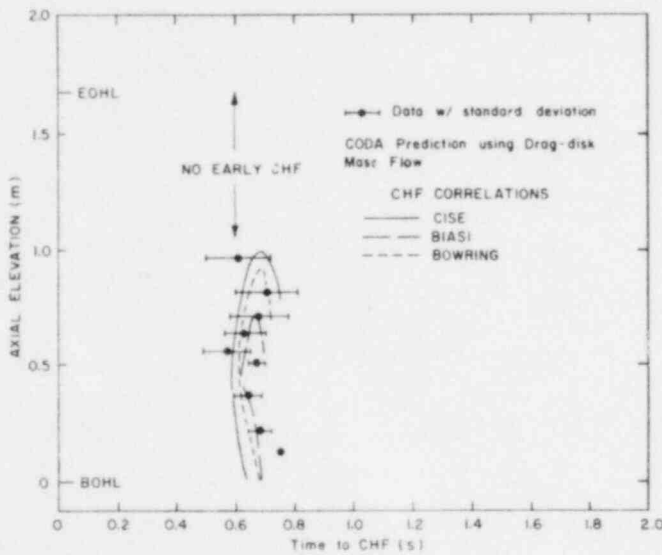
Fig. I.27

CHF Predictions Using Round-tube Correlations for Semiscale Test S-02-9. ANL Neg. No. 900-80-60.

Fig. I.28

CHF Predictions Using Rod-bundle Correlations for Semiscale Test S-02-9. ANL Neg. No. 900-80-57.
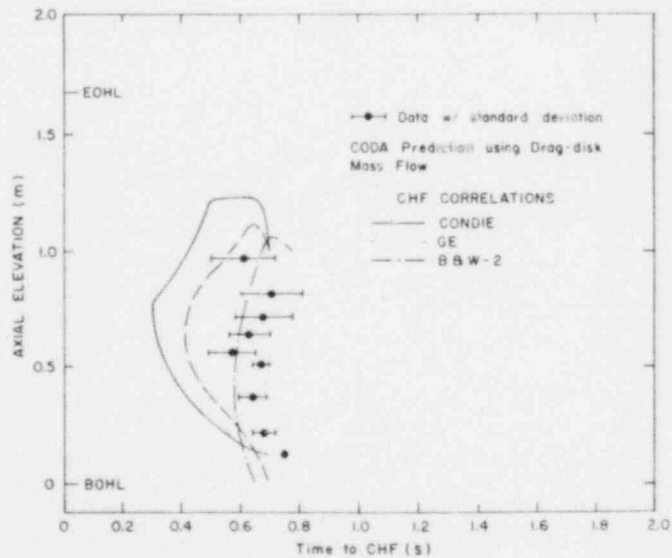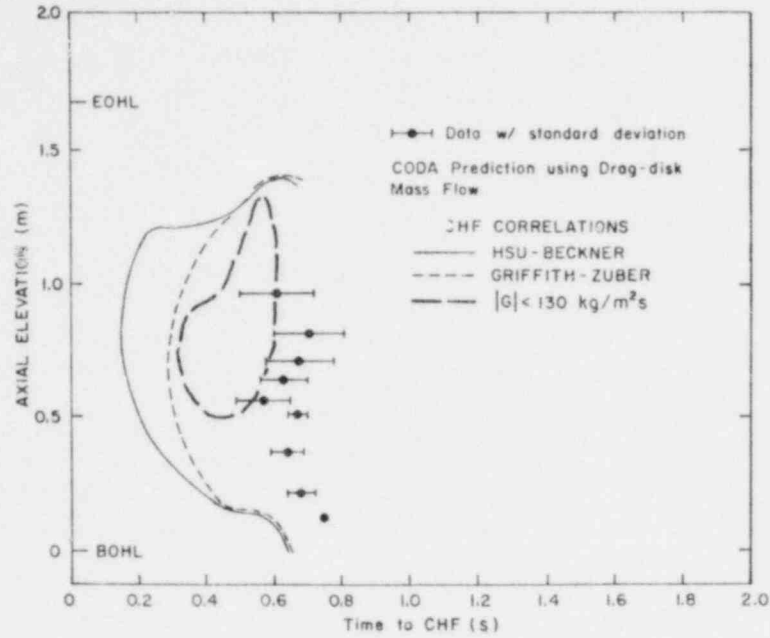
Fig. I.29. CHF Predictions Using Hsu-Beckner and Griffith-
Zuber Correlations for Semiscale Test S-02-9.
ANL Neg. No. 900-80-56.

This test had a further point of interest in that all thermo-
couples but three measured delayed CHF at about 4 s. The three that dem-
onstrated early CHF behavior were found in the high-power rods near the
lower one-third of the core, but they all subsequently measured rewet. During
blowdown, the flow direction was predominantly downward in the heated core.
In this test, only Griffith-Zuber, Hsu-Beckner, and Condie correlations pre-
dicted any CHF onset at all.

The CHF data shown in Fig. I.30 reveal that the high-power
rods experienced CHF slightly earlier than the low-power ones. In the cur-
rent CODA analysis, the supplied heat flux was a weighted average of the core
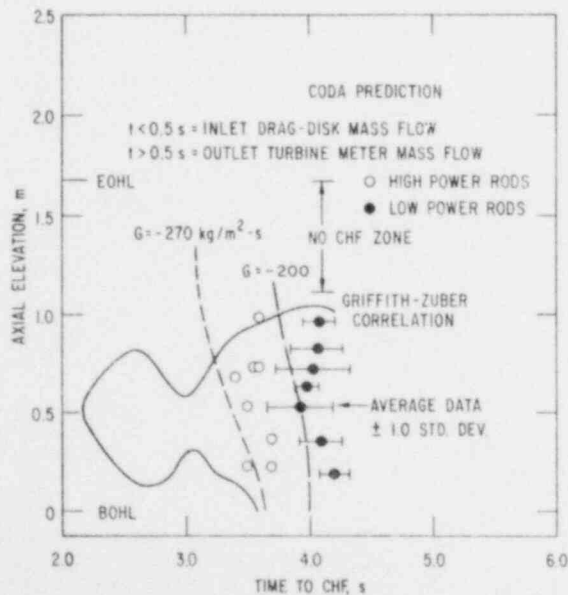
Fig. I.30

CHF Predictions Using Griffith-
Zuber Correlation for Semiscale
Test S-06-6: Case 1. ANL Neg.
No. 900-80-31 Rev. 1.

at each power level; hence no distinction between high- and low-power rods could be made. The results of the prediction should be interpreted with this limitation in mind. Two CODA calculations were made based on the following two cases of mass-flow-rate measurement:

> Case 1: Mass flow rate based on drag disk for t < 0.5 s and turbine meter for t > 0.5 s in combination with densitometer measurement.

> Case 2: Mass flow rate based on drag disk and densitometer throughout the transient.

Figures I.30 and I.31 illustrate the prediction of the Griffith-Zuber correlation for cases 1 and 2, respectively. The prediction is seen to be very conservative without imposing a mass-velocity criterion. Therefore the curves of two constant-mass velocities were drawn in both figures, and the one at -200 kg/m²·s can be seen to closely correlate the low-power rod data. With this criterion, the Griffith-Zuber correlation was able to do a remarkably good job of predicting both the extent and onset of CHF in this test. The Hsu-Beckner correlation yielded an adequate prediction, as shown in Fig. I.32. However, the predicted time was rather conservative. The Condie Mod-7 correlation in Fig. I.33 yielded good agreement with the CHF data also.
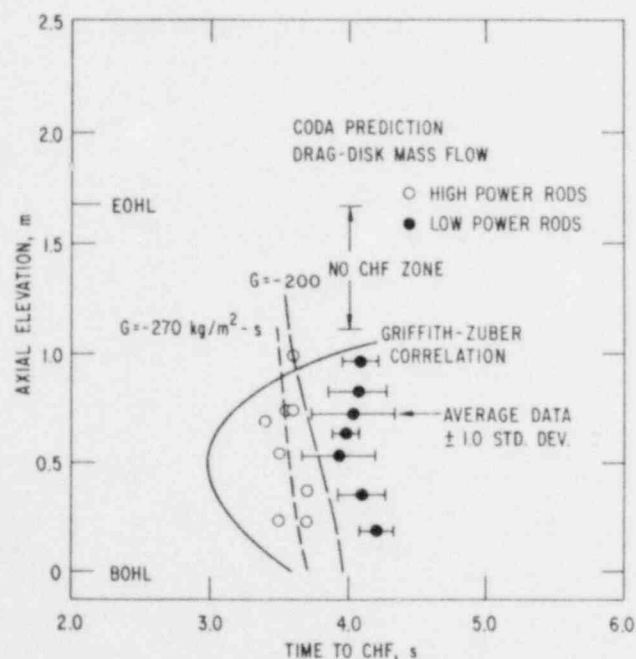
Fig. I.31. CHF Predictions Using Griffith-Zuber Correlation for Semiscale Test S-06-6: Case 2. ANL Neg. No. 900-80-30 Rev. 1.
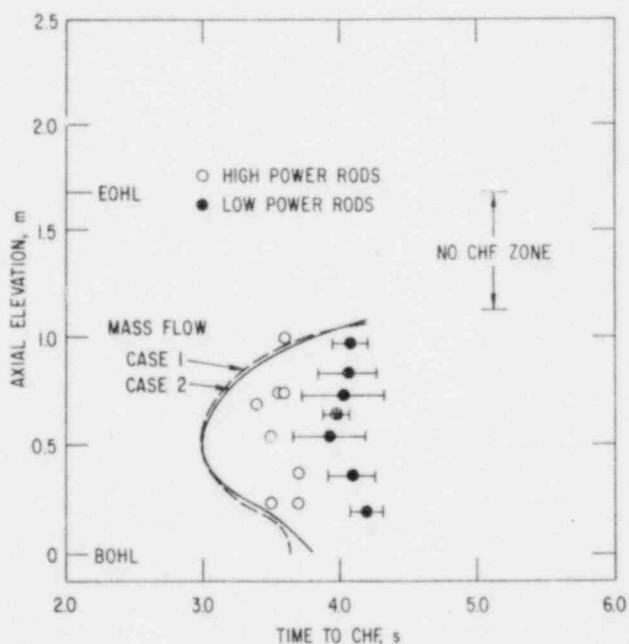
Fig. I.32. CHF Predictions Using Hsu-Beckner Correlation for Semiscale Test S-06-6. ANL Neg. No. 900-80-166.

22
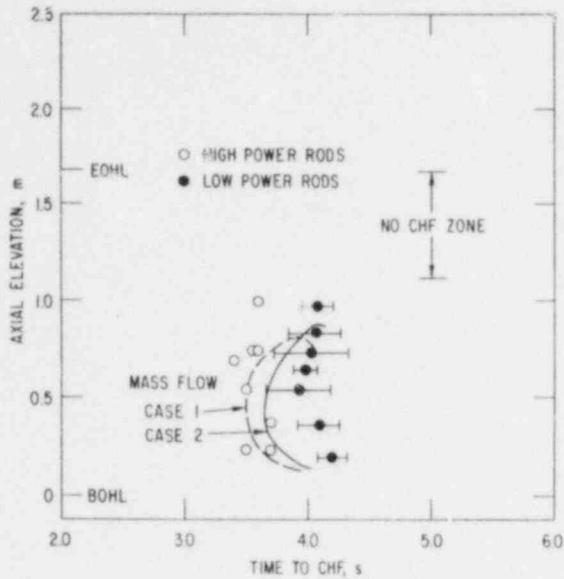
Fig. I.33

CHF Predictions Using Condie Mod-7
Correlation for Semiscale Test S-06-6.
ANL Neg. No. 900-80-167.

Test S-07-3 was conducted in the Mod-3 system with a full-length 5 x 5 PWR bundle. The initial conditions were[5]

$$P = 15.9 \text{ MPa},$$

$$T_{in} = 285°C,$$

$$W = 9.5 \text{ kg/s},$$

$$G_{in} = 3690 \text{ kg/m}^2 \cdot s \text{ (in core)},$$

and

$$q = 2.05 \text{ MW}.$$

Two corner rods were unpowered to simulate a control rod an an instrumented guide tube. The CODA calculation was performed using the core-inlet drag-screen mass flow as one of the hydraulic boundary conditions. The system pressure history was taken from pressure-transducer measurement at the upper plenum. The heat flux into the coolant was estimated as usual using the HETRAP inverse-heat-conduction code[20] with measured interior temperature and power history as input. Experimentally, CHF was first measured in the peak-heat-flux zone at about 0.6 s; the lowest level experienced overheating after quite some delay in time at about 1.5 s.

The round-tube correlations in Fig. I.34 predicted the CHF onset in the middle and upper portions of the core well, but underpredicted the time significantly in the bottom region. GE and B&W-2 correlations yielded similar results, as shown in Fig. I.35, whereas Condie correlation predicted the trend of the data well, but somewhat underpredicted the time. Both Hsu-Beckner and Griffith-Zuber correlations predicted CHF too early, as shown in Fig. I.36. The latter prediction could be improved slightly with a mass-flux criterion of $|G| < 130 \text{ kg/m}^2 \cdot s$ in the upper half of the core.
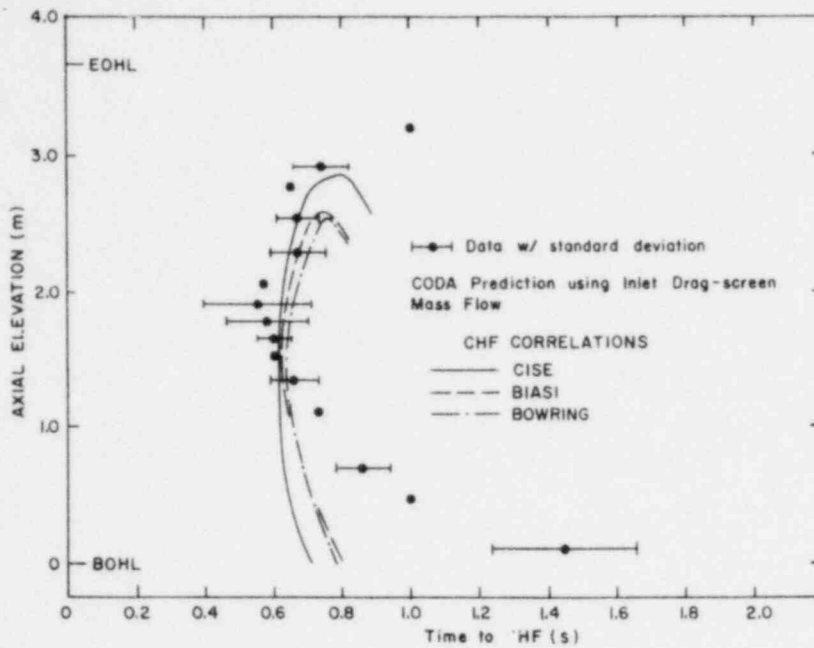
Fig. I.34. CHF Predictions Using Round-tube Correlations for
Semiscale Test S-07-3. ANL Neg. No. 900-80-58.
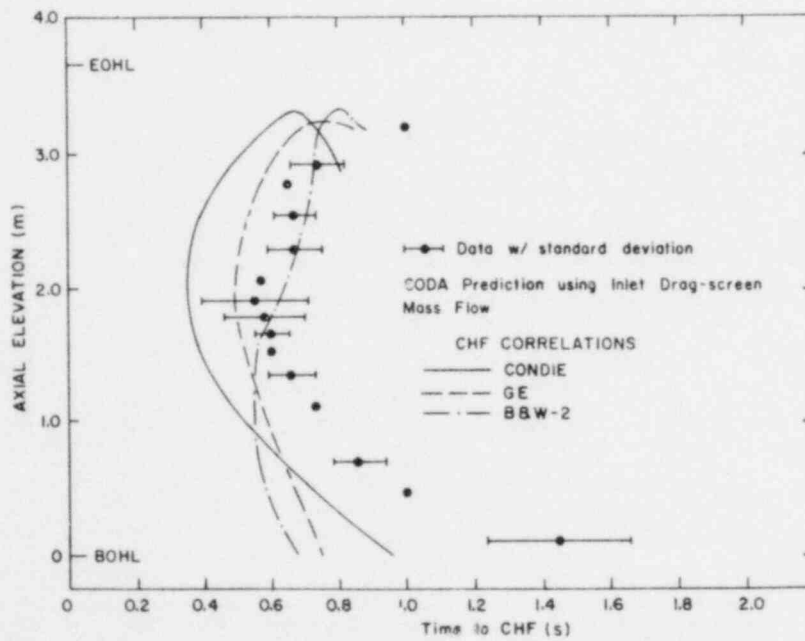
Fig. I.35. CHF Predictions Using Rod-bundle Correlations for
Semiscale Test S-07-3. ANL Neg. No. 900-80-61.
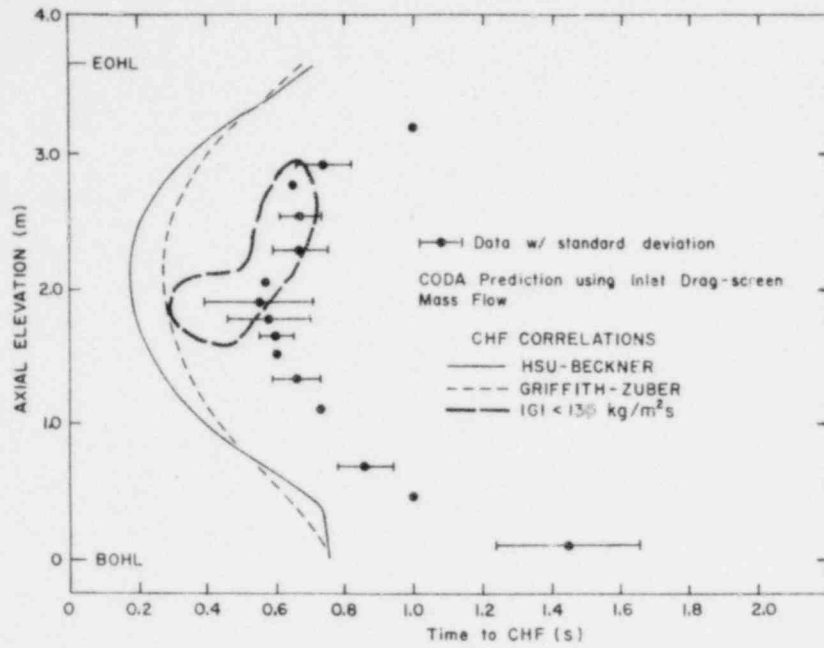
Fig. I.36. CHF Predictions Using Hsu-Beckner and Griffith-Zuber
Correlations for Semiscale Test S-07-3. ANL Neg.
No. 900-80-59.

c. Comments on CHF Correlations

The prediction results for the blowdown experiments are summarized in Table I.1. Note that all correlations received the same score for

TABLE I.1. Summary of Blowdown Heat Transfer Results

TESTS AND SPECIFICATIONS	BOWRING	BIASI	CISE	GRIFFITH -ZUBER	GE	CONDIE MOD-7	B&W-2	HSU- BECKNER	x = 1.0
CE/EPRI ROD-BUNDLE BHT-25	◯	◯	◯	◯	◯	◯	◯	◯	◯
LOFT COLUMBIA LOOP	◯	◯	◯	●	◯	○	◯	●	◯
PBF LOC-11C	●	●	●	◯	◯	◯	●	●	●
THTF BUNDLE #1									
TEST 105	○	◯	◯	○	◯	○	○	●	◯
TEST 104	◯	◯	◯	○	◯	○	○	●	◯
TEST 178	◯	◯	◯	○	◯	○	○	○	◯
TEST 181	○	◯	◯	○	◯	○	●	○	◯
TEST 177	●	◯	◯	◯	◯	○	●	○	◯
SEMISCALE MOD-1									
S-02-1	●	●	●	◯	●	●	●	○	●
S-02-9	○	◯	◯	●	○	○	◯	●	●
S-29-2	◯	○	◯	●	○	○	○	●	●
S-28-1 (EARLY AND DELAY CHF)	◯●	◯○	◯○	●◯	◯◯	○●	◯○	○●	●●
S-06-6	●	●	●	◯	●	◯	●	○	●
SEMISCALE MOD-3									
S-07-3	◯	◯	◯	●	◯	◯	◯	●	○
S-07-9	◯	◯	◯	●	○	○	○	●	○

NOTATION: ◯ GOOD PREDICTION; ○ ACCEPTABLE (USUALLY EARLY T_{CHF} PREDICTED); ● UNACCEPTABLE (MANY CASES NO CHF PREDICTION)

the GE rod-bundle test because none of them predicted CHF in agreement with test data. In general, the early CHF (t ≈ 1 s) was best predicted by the round-tube correlations, which are applicable over a wide range of pressures. In particular, CISE correlation has been demonstrated to correlate some limited steady-state rod-bundle CHF data well (Ref. 21). Biasi correlation is an equally good candidate; Bowring correlation is the least effective of the three. The B&W-2 correlation was obtained with mostly low-quality ($x < 0.2$) or DNB-type rod-bundle data at above 13.8 MPa. Therefore it would not be expected to work well under blowdown conditions that were definitely outside its range of applicability.

On the other hand, the Condie Mod-7 correlation was obtained with most of the available rod-bundle data (including both DNB and dryout data), and why it performed so marginally for the blowdown data is not at all clear. As a whole, it tends to correlate the delay CHF much better than the early ones. The GE low-flow correlation performed adequately for most of the early CHF data, but was found incapable in the prediction of delay CHF in Semiscale data.

The Hsu-Beckner correlation was actually derived empirically with blowdown data, but in the present study, this correlation was found inadequate and, in most instances, yielded very conservative predictions. Almost the same conclusion can be drawn about the Griffith-Zuber correlation; like the Hsu-Beckner correlation, it is strongly dependent on the bulk void fraction. However, if a mass-velocity criterion was proposed for its application, it was found to predict all the delay CHF very well. Based on the limited amount of data, it is tentatively recommended for the following range of mass velocity:

$$-240 < G < 100 \text{ kg/m}^2 \cdot \text{s.}$$

Keep in mind that this criterion is strongly affected by the reported mass flow and that mass velocity of this low magnitude is difficult to measure accurately in these experiments.

In general, the delay CHF was found to occur in a more tranquil state, at low and slowly decaying mass flow rate. One reason the round-tube correlations all failed in predicting this long-term CHF is simply that it occurs at the very low end of the applicable range of these correlations. In many instances, the early CHF can be well correlated by the $x = 1.0$ line, and this is certainly indicative of an annular-flow dryout-type phenomena. On the other hand, the delay CHF during blowdown occurred at well over 80% void fraction, and the success of the modified Zuber pool-boiling correlation suggests that CHF is caused by flooding and pool-boiling-type hydrodynamic crises.

During the recent Three Mile Island accident, the core over-heating occurred at about 100 min at less than 1% decay power. At such low heat-flux conditions, the applicability of the present CHF correlations would

be highly questionable. The overheating was brought about as the two-phase mixture level receded, uncovering the active core. Hence, in this situation, the hydrodynamic of the boil-up core plays a major role in determining the coolability of the fuel cladding. Therefore the conclusion and recommendations in the present study should best be made use of in large-break LOCA analyses.

References

1. J. C. M. Leung and K. A. Gallivan, "Transient Critical Heat Flux," Light-water-reactor Safety Research Program: Quarterly Progress Report, April-June 1979, ANL-79-81, NUREG/CR-1164 (Nov 1979).

2. Ibid., July-September 1979, ANL-79-108, NUREG/CR-1137 (Feb 1980).

3. M. L. Patton, Semiscale Mod-3 Test Program and System Description, TREE-NUREG-1212 (also NUREG/CR-0239) (1978).

4. Project Description: ORNL PWR Blowdown Heat Transfer Separate-Effects Program--Thermal-Hydraulic Test Facility (THTF), NUREG/CR-0104 (1978).

5. R. L. Gillins et al., Experiment Data Report for Semiscale Mod-3 Blow-down Heat Transfer Test S-07-3 (Baseline Test Series), NUREG/CR-0356 (1978).

6. D. H. Miyasaki et al., Experimental Data Report for Semiscale Mod-3 Blowdown Heat Transfer Test S-07-9 (Baseline Test Series), NUREG/CR-0815 (1979).

7. W. G. Craddick et al., PWR Blowdown Heat Transfer Separate-Effects Program--Thermal-Hydraulic Test Facility Experimental Data Report for Test 177, ORNL/NUREG/TM-295 (1980).

8. W. T. Hancox and S. Banerjee, Numerical Standards for Flow Boiling Analysis, Nucl. Sci. Eng. 64, 106 (1977).

9. D. M. Snider. Analysis of the Thermal-Hydraulic Behavior Resulting in Early Critical Heat Flux and Evaluation of CHF Correlations for the Semiscale Core, TREE-NUREG-1073 (1977).

10. C. L. Wheeler et al., COBRA-IV-I: An Interim Version of COBRA for Thermal Hydraulic Analysis of Rod Bundle Nuclear Fuel Elements and Cores, BNWL-1962 (1976).

11. V. D. Clemons et al., PWR Blowdown Heat Transfer Separate-Effects Program--Thermal-Hydraulic Test Facility Experimental Data Report for Test 105, ORNL/NUREG/TM-143 (1977).

12. L. J. Ott and R. A. Hedrick, ORINC--A One-Dimensional Implicit Approach to the Inverse Heat Conduction Problem, ORNL/NUREG-23 (Nov 1977).

13. D. M. Leon et al., *PWR Blowdown Heat Transfer Separate-Effects Program--Thermal-Hydraulic Test Facility Experimental Data Report for Test 104*, ORNL/NUREG/TM-152 (1978).

14. W. G. Craddick et al., *PWR Blowdown Heat Transfer Separate-Effects Program Data Evaluation Report--Heat Transfer for THTF Test Series 100*, ORNL/NUREG-45 (1978).

15. W. G. Craddick et al., *Quick Look Report on Thermal Hydraulic Test Facility Test 178*, ORNL/BDHT-2250 (Mar 21, 1979).

16. W. G. Craddick et al., *Quick Look Report on Thermal Hydraulic Test Facility Test 181*, CRNL/BDHT-2254 (Apr 26, 1979).

17. W. G. Craddick, ORNL, private communication (Oct 1979).

18. H. S. Crapo et al., *Experiment Data Report for Semiscale Mod-1 Tests S-02-9 and S-02-9A (Blowdown Heat Transfer Tests)*, ANCR-1236 (1976).

19. V. Esparza and K. E. Sackett, *Experiment Data Report for Semiscale Mod-1 Test S-06-6 (LOFT Counterpart Test)*, TREE-NUREG-1126 (1977).

20. S. Malang, *HETRAP: A Heat Transfer Analysis Program*, ORNL-TM-4555 (1974), available from National Energy Software Center at ANL.

21. J. C. M. Leung and R. E. Henry, *Prediction of CHF in Rod Bundles Using Round-tube CHF Correlation*, Trans. ANS 33, 963 (1979).

II. TRANSIENT FUEL RESPONSE AND FISSION-PRODUCT RELEASE

Principal Investigators
J. Rest and S. M. Gehl, MSD

A. Introduction and Summary

A physically realistic description of fuel swelling and fission-gas release is needed to aid in predicting the behavior of fuel rods and fission gases under certain hypothetical light-water-reactor (LWR) accident conditions. To satisfy this need, a comprehensive computer-base model, the Steady-state and Transient Gas-release and Swelling Subroutine (GRASS-SST), its faster-running version, FASTGRASS, and correlations based on analyses performed with GRASS-SST, PARAGRASS, are being developed at Argonne National Laboratory (ANL). This model is being incorporated into the Fuel-rod Analysis Program (FRAP) code being developed by EG&G Idaho, Inc., at the Idaho National Engineering Laboratory (INEL).

The analytical effort is supported by a data base and correlations developed from characterization of irradiated LWR fuel and from out-of-reactor transient heating tests of irradiated commercial and experimental LWR fuel under a range of thermal conditions.

B. Modeling of Fuel/Fission-product Behavior (J. Rest, MSD)

1. Update on GRASS-SST and FASTGRASS Model Development

a. Random Diffusion of Bubbles to Grain Faces

The version of the GRASS-SST code reported in Ref. 1 did not include the random diffusion of gas bubbles from the grains to the grain boundaries. The assumption used in this version of the code was that, for most situations of interest, the flux of gas from the grains to the grain faces could be described by the random diffusion of gas atoms and the biased (in a temperature gradient) migration of gas bubbles. This assumption seemed reasonable in light of the nature of the characterization of the bubble-size distribution used in GRASS-SST; each size class represents a spectrum of bubble sizes, so that the single gas-atom size class actually represents very small gas bubbles as well as gas atoms. Thus, the random diffusion of very small bubbles (atoms/bubble < 10) was, in effect, included in the analysis.

However, there are certain conditions in which this assumption breaks down and the random diffusion of gas bubbles makes an important contribution to the flux of gas from the grains to the grain faces. For example, in an isothermal environment under conditions of low linear power (such that the re-solution rate is negligible), the gas-atom population will rapidly disappear

due to the coalescence of the gas atoms into bubbles. Thus, under these conditions, unless the random diffusion of gas bubbles is considered, GRASS-SST will not allow any gas to reach the grain faces. Subsequent GRASS-SST analyses for isothermal, low-linear-power-type environments (e.g., TMI-2 accident scenarios, see Sec. 2 below) using the following formalism for the random diffusion of gas bubbles from the grains to the grain boundaries have demonstrated that this mechanism of bubble mobility is a key factor influencing gas release under these conditions.

The calculation of the rate at which fission-gas bubbles diffuse randomly to the grain faces has been included in GRASS-SST as follows. A time interval, h, is chosen such that the average distance a gas bubble moves is small compared to the average distance separating the bubbles (i.e., the bubbles do not interact), and such that bubble shrinkage due to re-solution can be neglected. Then, the equation describing the random diffusion of the gas bubbles is given by

$$\frac{\partial c_i}{\partial t} = D_i \nabla^2 c_i, \quad c_i = C_i^g \text{ at } r = a, \quad c_i = C_i^0 \text{ at } t = 0, \tag{1}$$

where c_i is the number of bubbles in the ith size class per unit volume of fuel, t is the time, D_i is the diffusivity of an i-size bubble, a is the grain radius, C_i^g is the concentration of i-size bubbles at $r = a$, and C_i^0 is the concentration of i-size bubbles within the grain at $t = 0$.

The solution of Eq. 1 yields c_i as a function of r (the distance from the center of the spherical grain) and the time t; thus,

$$c_i = C_i^g - \frac{2(C_i^0 - C_i^g)a}{\pi r} \sum_{m=1}^{\infty} \frac{(-1)^m}{m} \exp(-m^2\pi^2 D_i t/a^2) \sin(m\pi r/a). \tag{2}$$

Integrating the amount passing through the surface and dividing by the total amount initially in the sphere gives

$$F_i = 1 - \frac{6(C_i^0 - C_i^g)a}{\pi^2} \sum_{m=1}^{\infty} \frac{(-1)^m}{m} \exp(-m^2\pi^2 D_i t/a^2) \sin(m\pi r/a). \tag{3}$$

where F_i is the fraction of i-size bubbles diffused out of the sphere in time t. The infinite series in Eq. 3 converges rapidly for $\pi^2 D_i t/a^2 \geq 1$, and the first term only is an excellent approximation. Thus,

$$F_i = 1 - \frac{6(C_i^0 - C_i^g)}{\pi^2} \exp(-\pi^2 D_i t/a^2), \quad \pi^2 D_i t/a^2 \geq 1. \tag{4}$$

On the other hand, when $\pi^2 D_i t/a^2 \leq 1$, a good approximation to Eq. 3 is given by

$$F_i = 3(C_i^0 - C_i^g)\left[\frac{2}{a}\left(\frac{D_i t}{\pi}\right)^{1/2} - D_i t/a^2\right], \ \pi^2 D_i t/a^2 \leq 1. \tag{5}$$

At $\pi^2 D_i t/a^2 = 1$, both approximations are good. The rate, R_i, at which the i-size gas bubbles migrate randomly to the grain face at $r = a$ can then be obtained from Eqs. 3-5 by

$$R_i = \frac{dF_i}{dt}. \tag{6}$$

Note that the above equations only describe the flux of gas from the grains to the grain boundaries due to the random diffusion of bubbles. These equations (and those for the biased diffusion of bubbles from the grains to the grain boundaries) supplement the calculation of the bubble-size distribution functions in GRASS-SST that use relations describing the random and biased migration contributions to bubble coalescence as well as the formalism for gas-atom re-solution (e.g., see Ref. 1.).

b. Random Diffusion of Grain-face Bubbles to Grain Edges

The version of the GRASS-SST code reported in Ref. 1 did not include the random diffusion of gas bubbles from the grain faces to the grain edges. The assumption used in the code was that, for most situations of interest, the flux of gas from the grain faces to the grain edges could be described as random diffusion of gas atoms, the biased diffusion of gas bubbles, and grain-face channel formation. However, for completeness, the method of calculating the rate at which gas atoms diffuse randomly from the grain faces to the grain edges (see Ref. 1, Sec. II.F) has been generalized to include the calculation of the random diffusion rates for gas bubbles. This was accomplished directly by substituting the appropriate gas-bubble diffusivities and boundary concentrations in place of the gas-atom diffusivities and boundary concentrations in Eq. 50 of ANL-78-53 (i.e., Ref. 1).

2. GRASS-SST Analyses for TMI-2 Accident-type Conditions

a. Introduction

GRASS-SST analyses of fission-gas response for TMI-2 accident-type scenarios were performed in order to gain a perspective on the subsequent condition of the fuel. These analyses are intended to be qualitative due to the lack of hard data on the fuel transient temperatures and on any microstructural changes that might have occurred in the fuel as a consequence of the accident (e.g., extensive fuel fracturing). To best gain the insight required for an interpretation of the GRASS-SST-calculated results for these TMI-2 accident-type conditions, it is appropriate at this time to present a short discussion on the associated phenomenology.

GRASS-SST is a mechanistic computer code[1,2] for predicting fission-gas behavior in nuclear fuels. GRASS-SST treats fission-gas release and fuel swelling in an internally consistent manner and simultaneously treats all major mechanisms thought to influence fission-gas behavior. The GRASS-SST steady-state and transient analysis has evolved through comparisons of code predictions with the fission-gas release and physical phenomena that occur during both reactor operation and transient direct-electrical-heating (DEH) testing of irradiated light-water-reactor fuel.[3-5]

GRASS-SST calculations include the effects of the production of gas from fissioning uranium atoms, bubble nucleation, a realistic equation of state for xenon, bubble diffusivities based on experimental observations, bubble diffusion, bubble migration, bubble coalescence, gas-bubble/channel formation on grain faces, re-solution, temperature and temperature gradients, interlinked porosity, nonequilibrium effects, and fission-gas interaction with structural defects on both the distribution of fission gas within the fuel and on the amount of fission gas released from the fuel. GRASS-SST calculates the fission-gas-induced swelling due to, and the fission-gas-bubble-size distribution for, bubbles in the lattice, on dislocations, and on the grain boundaries, and the fission-gas release as a function of time, and the position within the fuel for steady-state and transient conditions. Fission gas released from the fuel reaches the fuel surface by successively diffusing from the grains to grain faces and then to the grain edges, where the gas is released through a network of interconnected tunnels of fission-gas and fabricated porosity.

The accumulation of fission gas (and other fission products) on grain faces and edges tends to degrade the strength of the boundary, and grain-boundary separation may result if the stresses on the boundary exceed the boundary fracture strength. Experimentally, a change in the mode of fuel fracture from predominantly intra- to intergranular has been observed[6] in high-burnup fuel irradiated at relatively low temperatures. Extensive grain-boundary separation has been observed[2,4,7] to occur during the DEH transient heating tests on irradiated commercial UO_2 fuel. A correlation has been noted between the increase in pore-solid interfacial surface area during these tests and the amount of fission gas released. SEM examination of the tested specimens indicates that intergranular separations can form by the diffusion-controlled processes of growth and coalescence of fission-gas bubbles. In addition, this gradual process of bubble growth and coalescence to form channels, and channel coalescence to form separations, can be interrupted by the more rapid process of crack propagation. Crack propagation results from stresses on weakened grain boundaries. The stresses responsible for cracking are the result of applied axial load, differential thermal expansion, solid fission-product swelling, and the pressurization of intergranular fission-gas bubbles. Grain-boundary separation has also been observed in fuel tested in the PBF reactor in Idaho, and in commercial fuel that had undergone a power excursion in the Dresden reactor in Illinois.

Thus, in order to accurately predict the release of fission gas from grain faces and edges, one must be able to calculate not only the evolution of the grain-edge porosity interconnection, but also the onset and the degree of grain-boundary separation. These two phenomena are somewhat interdependent in that they are both precipitated, in part, by the accumulation of fission gas. Whether one or the other or both phenomena occur is dependent on fuel type (e.g., grain size, density, etc.) as well as on the particular operating scenario under consideration.

At the present stage of development, GRASS-SST does not contain models for the formation and interlinkage of the planar intergranular separations observed in DEH-tested fuel, or for the type of extensive fuel fracturing that results from requenching stresses and observed in PBF tested fuel.[8] This latter type of fuel fracturing is thought to have occurred extensively in fuel subject to the accident at TMI-2.

b.　GRASS-SST Analyses

GRASS-SST analyses were performed for the portion of the calculated TMI-2 accident temperature scenario shown in Fig. II.1. These calculated temperatures represent an extreme, where nominal make-up flows and no reflux are assumed. The calculations were made for the fuel that reached the highest temperatures. Prior to these calculations, GRASS-SST was executed for the steady-state (~6-kW/ft) TMI-2 irradiation. The temperature history used for the as-irradiated condition is shown in the subgraph of Fig. II.1. Results of the GRASS-SST analysis for the 6-kW/ft TMI-2 fuel just before the initiation of the accident indicate that ~99% of the generated gas was still within the fuel grains.
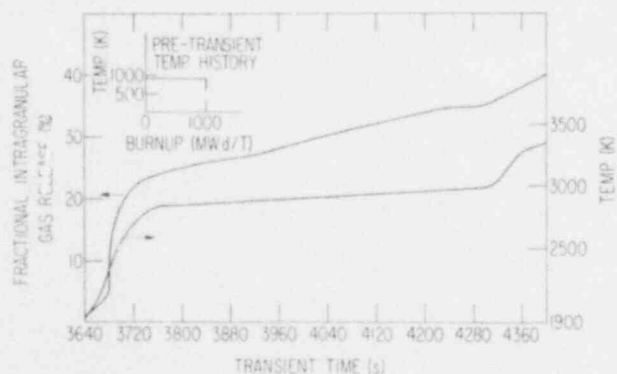
Fig. II.1

GRASS-SST-calculated Intragranular Transient Gas Release as a Function of Time after the First 100 min of a Calculated TMI-2 Accident Temperature Scenario

Figure II.1 shows GRASS-SST results for intragranular fission-gas release as a function of the transient time subsequent to the first 100 min of the accident. (Note that only the first 2.9 h of the transient has been simulated.) Also shown in Fig. II.1 is the temperature history used as input to the GRASS-SST calculations. The results indicate that at the end of the first 2.9 h of the transient, ~42% of the generated gas has migrated out of the fuel grains to the grain faces and edges and is available to be released in the advent of

extensive fuel fracturing. (If no fuel fracturing occurs, GRASS-SST predicts that this released intragranular fission gas remains trapped on the grain faces and grain edges; i.e., no extensive interlinkage of the grain-face channels and the grain-edge tunnels is predicted to occur.)

The model for intragranular gas-bubble diffusivity used in the GRASS-SST code[1,2] is unique in the sense that it relates the bubble diffusivity to the fuel yield stress, heating rate, and vacancy mobility, as well as to fuel temperature and bubble radius. Figures II.2 and II.3 show the results of analyses performed with GRASS-SST for three values of the fuel heating rate (5, 10, and 25°C/s), two values for the initial fuel temperature (650 and 1500°C), and two values for the final fuel temperature (2000 and 2650°C). The as-irradiated history is the same as shown in the subgraph of Fig. II.1 with the addition of a mild heat up to 650°C (Fig. II.2) and 1500°C (Fig. II.3) before the initiation of the heating rate ramps. For each value of the initial fuel temperature and for each heating ramp, two final fuel temperatures were used. These final fuel temperatures were then held constant for an additional 5 h in order to be able to compare the predicted intragranular release during the heating-rate ramp and during a constant (high)-temperature period.
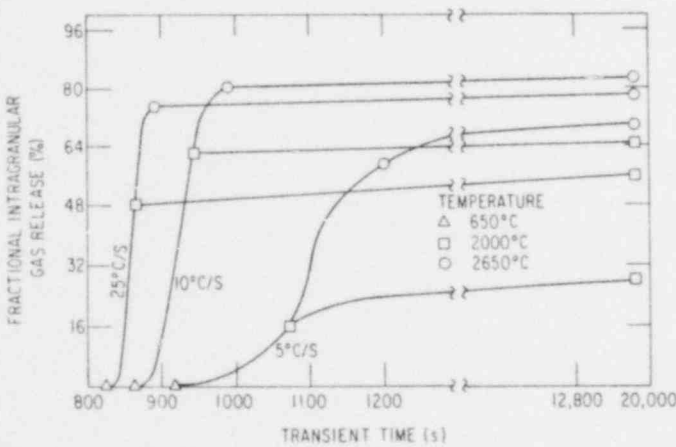
Fig. II.2

GRASS-SST-calculated Intragranular Transient Gas Release for Several Fuel-temperature and Heating-rate Scenarios with a Starting Temperature of 650°C

Fig. II.3

GRASS-SST-calculated Intragranular Transient Gas Release for Several Fuel-temperature and Heating-rate Scenarios with a Starting Temperature of 1500°C
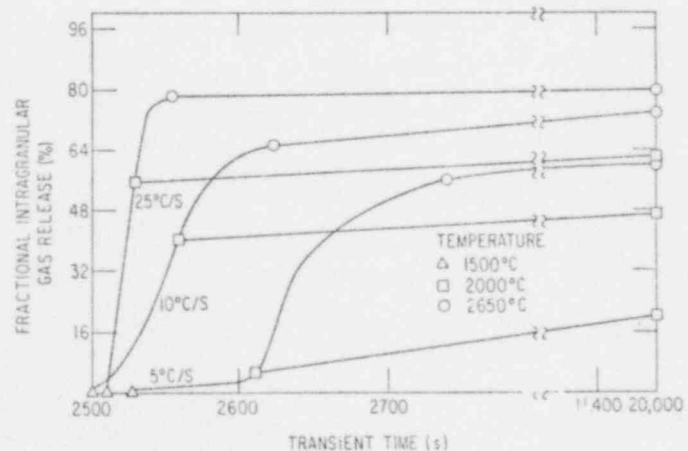
Observation of Figs. II.2 and II.3 leads to the following conclusions:

(1) The greater the difference between the initial and final fuel temperatures, the greater the predicted intragranular gas release.

(2) Although there is an initial trend of increased intragranular gas release with increased heating rate, an increase in heating rate above a specified value leads to a decrease in the predicted intragranular gas release. For example, the 10°C/s ramp results in a higher predicted release than the 25°C/s ramp, as shown in Fig. II.2. The value of heating rate that results in the maximum predicted gas release depends on the initial and final temperatures as can be seen by comparing Figs. II.2 and II.3 (i.e., in Fig. II.3, the 25°C/s ramp results in the highest predicted intragranular gas release).

(3) Most of the intragranular gas release is predicted to occur during the heating-rate ramp; only a minor increase in the predicted release occurs during the high-temperature, 5-h period, as shown in Figs. II.2 and II.3.

Thus, based on these analyses, if a substantial release of fission gas resulted as a consequence of the first 3 h of the accident at TMI-2, the following observations follow:

The gas-bubble mobilities during some portion of the first 3 h must have been significantly higher (many orders of magnitude) than the diffusivities based on measurements made during similar isothermal conditions. Whether these mobilities resulted from a rapid heatup of the fuel, or from changes in stoichiometry, or both, or from some other unknown phenomenon is open to speculation at this time. In addition, extensive fuel fracturing must have occurred, enabling the gas that had reached the grain boundaries to vent to the exterior of the fuel.

References

1. J. Rest, GRASS-SST: A Comprehensive, Mechanistic Model for the Prediction of Fission-gas Behavior in UO_2-base Fuels during Steady-state and Transient Conditions, NUREG/CR-0202, ANL-78-53 (June 1978).

2. J. Rest and S. M. Gehl, The Mechanistic Prediction of Transient Fission-gas Release from LWR Fuel, Nucl. Eng. Design 56(1), 233-256 (Feb 1980)

3. J. Rest, M. G. Seitz, S. M. Gehl, and L. R. Kelman, "Development and Experimental Verification of SST-GRASS: A Steady-state and Transient Fuel Response and Fission-Product Release Code," Proc. CSNI Specialists Meeting on Behavior of Water Reactor Fuel Elements under Accident Conditions, Spatind, Norway (Sept 13-16, 1976).

4. S. M. Gehl, M. G. Seitz, and J. Rest, "Relationship Between Fission-Gas Release and Microstructural Change During Transient Heating of Pressurized Water Reactor Fuel," Proc. ANS Topical Meet. Thermal Reactor Safety, 1977, CONF-770708, Vol. 3, pp. 3-261 to 3-282 (July 31-Aug 5, 1977).

5. J. Rest, M. G. Seitz, and S. M. Gehl, Release of Fission Gas from High-Burnup Fuel During Transient Heating, Trans. Am. Nucl. Soc. 26, 320-324 (1977).

6. R. G. Bellamy and J. B. Rich, Grain-Boundary Gas Release and Swelling in High Burnup Uranium Dioxide, J. Nucl. Mater. 33, 64-76 (1969).

7. S. M. Gehl, M. G. Seitz, and J. Rest, Fission-gas Release from Irradiated PWR Fuel during Simulated PCM-type Accidents: Progress Report, NUREG/CR-0088, ANL-77-80 (May 1978).

8. A. W. Cronenberg and T. R. Yackle, An Assessment of Intergranular Fracture with Unrestructured UO_2 Fuel due to Film Boiling Operation, EG&G Idaho, Inc., NUREG/CR-0595, TREE-1330 (Mar 1979).

Distribution for NUREG/CR-1460 (ANL-80-43)

Internal:

R. P. Anderson
R. Avery
E. S. Beckjord
M. Blander
Y. S. Cha
H. M. Chung
L. W. Deitrich
C. E. Dickerman
B. R. T. Frost
S. M. Gehl
E. E. Gruber
J. R. Honekamp

M. Ishii
W. D. Jackson
T. F. Kassner (24)
A. B. Krisciunas
J. A. Kyger
J. C. Leung
Y. Y. Liu
P. A. Lottes
W. E. Massey
L. McUmber
L. A. Neimark
R. G. Palm
D. R. Pepalis

R. B. Poeppel
L. J. Reinsch
J. Rest (30)
D. Stahl
E. M. Stefanski
R. P. Stein
W. Wang
R. W. Weeks
F. L. Yaggee
ANL Contract File
ANL Libraries (5)
TIS Files (6)

External:

NRC, for distribution per R2, R3, R4 (560)
DOE-TIC (2)
Manager, Chicago Operations and Regional Office, DOE
Chief, Office of Patent Counsel, DOE-CORO
President, Argonne Universities Association
Reactor Analysis and Safety Division Review Committee:
    S. Baron, Burns and Roe, Inc.
    J. R. Dietrich, Combustion Engineering, Inc.
    W. Kerr, U. Michigan
    M. Levenson, Electric Power Research Inst.
    S. Levy, S. Levy, Inc.
    D. Okrent, U. California, Los Angeles
    N. C. Rasmussen, Massachusetts Inst. Technology
Materials Science Division Review Committee:
    E. A. Aitken, General Electric Co., Sunnyvale
    G. S. Ansell, Rensselaer Polytechnic Inst.
    R. W. Balluffi, Massachusetts Inst. Technology
    R. J. Birgeneau, Massachusetts Inst. Technology
    S. L. Cooper, U. Wisconsin
    C. Laird, U. Pennsylvania
    M. T. Simnad, General Atomic
    C. T. Tomizuka, U. Arizona
    A. R. C. Westwood, Martin Marietta Labs.
R. B. Adamson, General Electric Co., Vallecitos Nuclear Center, P. O. Box 460, Pleasanton, Calif. 94566
R. Blomquist, Technical Inst., Northwestern University, Evanston, Ill. 60202
J. Boulton, Whiteshell Nuclear Research Establishment, AECL, Pinawa, Manitoba, R0E 1L0, Canada
D. L. Burman, Westinghouse PWR Systems Div., P. O. Box 355, Pittsburgh, Pa. 15230
R. H. Chapman, Oak Ridge National Lab., P. O. Box X, Oak Ridge, Tenn. 37830
M. Charyulu, EG&G Idaho, Inc., P. O. Box 1625, Idaho Falls, Idaho 83401
F. D. Coffman, Div of Operating Reactors, U. S. Nuclear Regulatory Commission, Washington
S. Dagbjartson, EG&G/INEL, 1520 Sawtelle Dr., Idaho Falls, Idaho 83401
J. Dearien, EG&G/INEL, 1520 Sawtelle Dr., Idaho Falls, Idaho 83401
D. Hagrman, EG&G/INEL, 1520 Sawtelle Dr., Idaho Falls, Idaho 83401
R. R. Hobbins, EG&G/INEL, 1520 Sawtelle Dr., Idaho Falls, Idaho 83401
D. O. Hobson, Oak Ridge National Lab., P. O. Box X, Oak Ridge, Tenn. 37830

W. V. Johnston, U. S. Nuclear Regulatory Commission, Washington

K. R. Jordan, Nuclear Fuel Div., Monroeville Nuclear Center, Westinghouse Electric Corp., Monroeville, Pa. 15146

P. MacDonald, EG&G/INEL, 1520 Sawtelle Dr., Idaho Falls, Idaho 83401

S. McDonald, Westinghouse Electric Corp. R&D Center, Beulah Rd., Pittsburgh, Pa. 15235

K. R. Merckx, Exxon Nuclear, Inc., 2955 George Washington Way, Richland, Wash. 99352

R. Mulgreen, Office of Nuclear Regulatory Research, U. S. Nuclear Regulatory Commission, Washington (3)

D. R. O'Boyle, Commonwealth Edison Co., P. O. Box 767, Chicago, Ill 60690

H. Ocken, Electric Power Research Inst., P. O. Box 10412, Palo Alto, Calif. 94304

R. N. Oehlberg, Electric Power Research Inst., P. O. Box 10412, Palo Alto, Calif. 94304

T. P. Papazoglou, Lynchburg Research Center, Babcock & Wilcox, P. O. Box 1260, Lynchburg, Va. 24505

M. Picklesimer, U. S. Nuclear Regulatory Commission, Washington

D. Powers, Div. of Systems Safety, U. S. Nuclear Regulatory Commission, Washington

W. J. Quapp, EG&G/INEL, 1520 Sawtelle Dr., Idaho Falls, Idaho 83401

C. Ronchi, Euratom - T.V., Postfach 2266, 75 Karlsruhe, West Germany

P. Smerd, Combustion Engineering, Inc., P. O. Box 500, Windsor, Conn. 06095

V. W. Storhok, Battelle Columbus Labs., 505 King Ave., Columbus, O. 43201

R. A. Watson, Carolina Power and Light Co., P. O. Box 1551, Raleigh, N. C. 27602